ABSTRACT

VASUDEO, NIKHIL BABURAM. The Regime Diagram for Premixed Flame Kernel-Vortex Interactions - Revisited. (Under the direction of Dr. Tarek Echekki).

Regimes of flame kernel-vortex (KV) interactions are investigated numerically using a detailed mechanism for hydrogen chemistry. The parametric simulations explore a wide range of conditions that are representative of conditions encountered at various degrees of turbulence intensity. The results show that KV interactions can be classified into five different regimes, which include 1) the laminar kernel regime, 2) the wrinkled kernel regime, 3) the breakthrough regime, 4) the global extinction regime, and 5) the regeneration after global extinction (RGE) regime. With the exception of the last regime, the transition from one regime to another in the order listed corresponds to increasing the vortex size and strength. Operation at the RGE regime reveals interesting dynamics of the flame front that results in reignition or mending of combustion regimes after most of the original kernel has extinguished due to intense straining. Two different types of combustion zones are observed, which correspond to a flamelet structure as well as to more diffuse structures of merged flame segments. A revised regime diagram of the KV interactions is proposed that includes the broader range of KV interactions and incorporate the new RGE regime.

The Regime Diagram for Premixed Flame Kernel-Vortex Interactions - Revisited

by
Nikhil Baburam Vasudeo

A thesis submitted to the Graduate Faculty of
North Carolina State University
in partial fulfillment of the
requirements for the degree of
Master of Science

Mechanical Engineering

Raleigh, North Carolina

2009

APPROVED BY:

_____	_____
Dr. Kevin Lyons	Dr. William Roberts

_____
Dr. Tarek Echekki
Committee Chair

DEDICATION

To my parents for their love and support.

BIOGRAPHY

Nikhil Vasudeo was born in Mumbai, India on November 14, 1984. He received his Bachelor of Engineering degree in Mechanical Engineering from Mumbai University in May 2006. In order to continue his education, he joined Graduate Program in Mechanical Engineering at North Carolina State University in 2007.

ACKNOWLEDGMENTS

For his constant guidance and support throughout the research, I would like to thank my advisor Dr. Tarek Echekki. He made me understand how to analyze the big picture of the research and then gradually move down to its nuances. This thesis would not have been possible without his expertise, insight and enthusiasm.

I would like to sincerely thank Dr. William Roberts and Dr. Kevin Lyons for taking time off their busy schedules and serving on my advisory committee. I would like to express gratitude towards Dr. Marcus Day and Dr. John Bell for providing the AMR code.

Special thanks to my roommates *anna* and *motu*, for providing never ending supplies of *rasam* and *pav-bhaji*. I would like to thank all my friends, especially Nandan, Vinay, Jai, Sneha and Shraddha, for being there for me and lending me their support.

Last but not the least; I would like to thank my parents and my family, for all that they have done for me. To them I dedicate this thesis.

TABLE OF CONTENTS

Chapter 6 Conclusions and Recommendations

LIST OF TABLES

Chapter 2

LIST OF FIGURES

Chapter 2

Chapter 3

Chapter 4

Chapter 5

CHAPTER 1

Introduction

This chapter discusses a few of the earlier works relevant to the present problem, which concerns the process of kernel-vortex (KV) interactions in premixed flames. The motivation behind the present work, the objectives and finally an outline of the thesis are presented in the introduction.

1.1 Related work and motivation

Turbulence naturally occurs in many flows of technological interest. It is described as the presence of small scale random fluctuations, which combine to form organized motion on large to small scales. Turbulent motion is observed in internal combustion engines as a result of the intake and exhaust through the valves and the cylinder geometry. Inlet and outlet valves, piston head and the combustion chamber of the internal combustion engines are designed such that they enhance turbulence, which results in high degree of mixing (Choi et al. 2000). Several chemical reactions take place, which occur over wide range of time scale varying from 10^{-8} seconds to 10 seconds. These reactions take place in reaction zones, which are stretched, broken and mended as the vortices interact with the flame. The presence of vorticity is an important feature of turbulence. Extensive research has shown that turbulent combustion is a process of continuous distortion, production and dissipation of the flame surface by vortices of various scales. It incorporates highly complicated physical phenomena

of combustion and turbulent flows. Other subjects like, thermo-diffusive instabilities, gas dynamics, chemical kinetics are also woven into them. This results in several challenges that surface when experiments and computations of turbulent combustion problems are carried out. In order to understand the process of turbulent combustion, simplified models such as flame-vortex configuration and kernel-vortex (KV) configurations are used.

1.1.1. Flame-vortex interaction

The goal of the flame-vortex interaction is to simulate turbulent combustion on a fundamental level. Flame-vortex interactions are very useful in analyzing the evolution of flame surfaces when vortices are impinged on them. It serves as a more realistic model of turbulent interactions as it simulates unsteady stretch-strain conditions on the flame. Basic mechanism of flame-vortex interactions consist of convecting a counter rotating vortex pair towards a flame front, and allowing them to interact with each other. Although flame fronts and vortices are essentially three-dimensional in space, a simplified flow field (consisting of vortices symmetric along their rotational axis) and a simplified flame (propagating through a uniform reactant mixture) is used to generate a two dimensional (planar) model. Various turbulent interactions, such as localized interaction of small fluid structures, can be observed with such a configuration (Rutland and Trouvé, 1993).

1.1.2. Kernel-vortex interaction

Laminar flame kernel-vortex (KV) interactions have been proposed as a canonical problem for a broad range of practical combustion applications by Eichenberger and Roberts (1999), Xiong et al. (2001) and Xiong and Roberts (2002). This configuration is essentially different from the flame-vortex configuration as it takes into account the mean curvature of the expanding kernel. The kernel-vortex configuration generates conditions for positive and negative curvature, which helps in studying the effects of unsteady stretch caused by vortices on it. Echekki et al. (2007) studied the effects of strain and curvature on the radical species of premixed methane-air mixture. They showed that species that diffuse at a rapid rate (H) are highly correlated to curvature than the species that diffuse less (CO). Kernel-vortex interactions also provide the capability of studying the stretch-strain effects of the same-vortex when it is interacted with kernel of different sizes. Also, these interactions, along with varied stretch conditions, generate scenarios where upstream and downstream flame-flame interactions are observed.

Inside a spark-ignition engine, the nascent flame kernel is subject to a full range of turbulent scales in addition to the large scale motions of tumble and swirl. These scales serve to enhance the rate of volumetric heat release through the enhancement of the turbulent flame surface area. The same configuration also bears some important relevance to the modeling of turbulent premixed flames, as shown by Echekki et al. (2006), as well including the involvement during KV interaction of a broad range of interactions that are relevant to high intensity turbulence conditions.

During KV interaction, a post-ignition premixed flame kernel is subject to the wrinkling and straining action of vortical structures resulting in different regimes of interactions. These regimes have been studied experimentally by Eichenberger and Roberts (1999), Roberts and Drake (2001) and Xion and Roberts (2002) and computationally by Kolera-Gokula and Echekki (2006) and Echekki and Kolera-Gokula (2007). These regimes include 1) the laminar kernel regime where the vorticity is weak to alter the shape or dynamics of the flame kernel, 2) the wrinkled kernel regime, which is characterized by extensive distortion of the flame kernel but eventually dissipate within its body, 3) the breakthrough regime where the vorticity has sufficient strength to punch through the flame kernel, and 4) the global extinction regime, which is characterized by a global straining of the flame kernel resulting in its extinction.

Recently, a regime diagram for KV interaction has been constructed by Echekki and Kolera-Gokula (2007) based on two key parameters that control the transition between the different regimes. These parameters correspond to, the ratio of the vortex strength to the laminar flame speed and the ratio of the vortex radius to the flame kernel radius at the onset of interactions. The diagram was constructed using direct numerical simulations and a simple two-step global mechanism, which is designed to capture the dynamics of lean methane-air flames. Although, the diagram was able to highlight the conditions of the various regimes that have been identified experimentally, a number of outstanding questions remain. The first is related to the extent of the role played by instabilities, in particular thermo-diffusive instabilities, in delineating the various regimes of KV interaction. The second, which is addressed here, is the extent complex chemistry plays in delineating regimes or creating different regimes as

well. By complex chemistry, we are interested primarily in the role played by the different layers in a premixed flame in response to the imposed straining and wrinkling effects of the vortex. Associated with these layers, including those in the reaction zone, may be a broad range of length and time scales, which may respond differently to an externally-imposed flow field.

1.2 Objective

The role of different scales within the reaction zone has been observed in a number of studies in the literature. For example, the apparent robustness of flames against imposed strain rate conditions helped extend the boundaries of the flamelet regime to include the "thin-reaction-zones" regime, as shown by Peters (1999). However, there should be a limit beyond which the flamelet structure of turbulent flames may not be sustained; but, would that transition evolve into a distributed reaction regime or to a fundamentally different mode? For non-premixed flames, there is evidence of flame shredding under intensely wrinkled flame (IWF) condition, as studied by Ratner et al. (2000); but, more experimental and numerical evidence is needed to establish equivalent conditions for premixed IWFs if they exist. Establishing this evidence is not necessarily a principal objective of the present study; however, an important scope is to explore a more intense subset of KV interactions, which may provide insight into the mechanisms of combustion under intense turbulence conditions.

The objective of the present study is three-fold 1) investigate any apparent distinction between simpler and more complex descriptions of chemistry and explore a broader range of

KV interactions, 2) identify any new regimes of KV interactions, and 3) construct a revised regime diagram for KV interactions that takes into consideration the effects of complex chemistry. The study is implemented using parametric simulations of KV interaction for a broad range of vortex strength and sizes for primarily stoichiometric conditions of hydrogen in O_2/N_2 mixtures.

1.3 Outline

The rest of the document is divided into five chapters.

- In Chapter 2, the numerical implementation, solution scheme and simulation conditions are discussed. Under numerical implementation the governing equations are presented. Boundary conditions and the vortex pair initialization have been discussed under solution scheme. Chemical mechanism, problem set-up, and mixture proportions have been discussed in simulation conditions.
- In Chapter 3, results of four combustion regimes (laminar kernel, wrinkled kernel, breakthrough, and global extinction) are discussed. These interactions are carried out for stoichiometric conditions.
- Chapter 4 presents the novel regime (regeneration after global extinction), which has been identified in this study. A single case with non-stoichiometric (equivalence ratio = 0.5) condition in which regeneration regime has been identified is also discussed.

- Chapter 5 proposes the new regime diagram in which all the five combustion regimes are shown.
- Chapter 6 discusses the conclusions where results are summarized for the interactions considered, along with recommendation for future work.

CHAPTER 2

Numerical Implementation and Simulation Conditions

This chapter discusses the numerical methodology, problem set-up and various parameters associated with KV interactions. A discussion of governing equations, boundary conditions, mixture proportions and chemical mechanism is presented below. They are followed by description of problem set-up, the domain of the solution and a list of simulation conditions. Finally, the parameters that affect KV interaction are discussed.

2.1 Numerical implementation and governing equations

The simulations are based on the low Mach number formulation of the reacting flow equations, developed by Rehm et al. (1978), with adaptive mesh refinement (AMR), developed by Day and Bell (2000, 2009). In this methodology, fluid is treated as a mixture of perfect gases. Soret, Dufour, radiative transport and gravity effects are ignored. With these assumptions, the governing equations for low Mach number formulations are:

- The conservation of momentum:

$$\frac{\partial \rho \mathbf{u}}{\partial t} + \nabla \cdot (\rho \mathbf{u}\mathbf{u}) = -\nabla \pi + \nabla \cdot \tau \tag{2.1}$$

- The conservation of energy:

$$\frac{\partial \rho h}{\partial t} + \nabla \cdot (\rho \mathbf{u} h) = \nabla \cdot \left(\frac{\lambda}{c_p} \nabla h \right) + \sum_{i=1}^{N} \nabla \cdot \left[h_i \left(\rho D_i - \frac{\lambda}{c_p} \right) \nabla Y_i \right] \tag{2.2}$$

- The conservation of species:

$$\frac{\partial \rho Y_k}{\partial t} + \nabla \bullet (\rho \mathbf{u} Y_k) = \nabla \bullet \left(\rho D_k \nabla Y_k \right) - \dot{\omega}_k \tag{2.3}$$

- The equation of state:

$$p_0 = \rho R_u T \sum_{i=1}^{N} \frac{Y_i}{W_i} \tag{2.4}$$

In the above equations, ρ is the density; **u** is the velocity vector; h is the mixture enthalpy; T is the temperature; Y_k is the mass fraction of the kth species in the mixture; W_k is the molecular weight of the kth species in the mixture; ω_k is the net destruction rate for species k due to chemical reactions; M is the Mach number; R_u is the universal gas constant; τ is the stress tensor; λ is the thermal conductivity; and $h_i(T)$ and D_i are the enthalpy and species mixture-averaged diffusion coefficient of ith species respectively; π (x, t) is the perturbational pressure, given by, π (x, t) = $p(x, t) - p_0(t)$, where p_0 is the ambient pressure. The equation of state for a perfect gas mixture (2.4) supplements the evolution equations (2.1)-(2.3).

2.2 Solution scheme

2.2.1 Boundary Conditions

For all quantities, the inlet boundary conditions are Dirichlet boundary conditions. They are applied directly on the face of the cell on the domain boundary. The integration scheme is based on a parallel adaptive mesh refinement framework, which uses a hierarchical system of rectangular grids. The scheme is second order accurate in space and time. It also conserves mass and enthalpy of the species.

2.2.2 Initialization of the vortex pair

The numerical configuration is shown in Fig. 2.1. A counter rotating vortex pair is initialized by using an Oseen vortex model. The tangential velocity, u_θ, for each vortex is given by

$$u_\theta = \begin{cases} \dfrac{\psi}{2\pi r}\left[1-\exp\left(-\dfrac{r^2}{\sigma^2}\right)\right], r \le \sigma \\ 0, r > \sigma \end{cases} \quad \text{where } r = \sqrt{\left(x-x_0\right)^2+\left(y-y_0\right)^2} \tag{2.5}$$

In this expression, σ is the vortex core radius; the coordinate (x_0, y_0) corresponds to the center location of each vortex. The parameter R_v, corresponds to the radial span of the vortex pair as shown in the figure. In general, σ and R_v are two independent parameters. However, in the present study, the distance between the centers of the two vortices is set to 0.2 cm; and therefore, the effective vortex pair radius is expressed as: $R_v = \sigma + 0.1$ cm. The vortices are set at equal distance relative to the vertical symmetry axis, as shown in Fig. 2.1. ψ is the vortex strength, which can be expressed in terms of maximum tangential velocity, $u_{\theta,\max}$, as follows:

$$\psi = u_{\theta,\max}\sigma\left[\frac{2\pi}{1-e^{-1}}\right] \approx 9.9399 u_{\theta,\max}\sigma \tag{2.6}$$

2.3 Simulation Conditions

Parametric simulations are implemented by varying the vortex strength, $u_{\theta,\max}$, and size, R_v. The bulk of the simulations are based on a uniform stoichiometric mixture of $H_2/O_2/N_2$ with proportions of N_2 to O_2 being 6.35 by volume, respectively. However, we also present a

case in the results where the equivalence ratio is 0.5 and the proportion of N_2 to O_2 the same as in the stoichiometric cases. Radiative losses and gravity forces are neglected. The simulations are performed on 3 × 4 cm domain; the longer dimension corresponds to the direction of the vortex pair displacement as shown in Fig. 2.1. The base grid in the *x* and *y* directions is 96 by 128 respectively, with two levels of refinements included to resolve the flame and the vortex structure. The center of the flame kernel (i.e. the ignition point) is chosen as 1.5 cm above the base, and the center of the vortex pair is chosen to as 1.2 cm from the base. Therefore, the distance between the two centers is fixed for all cases considered at 0.3 cm.

Although the effect of the initial separation distance between the centers of vortex and kernel can be studied, in this work, the primary focus is on the effects of vortex size and strength on the expanding kernel. As stated earlier, the distance between the centre of the vortex and the axis of symmetry has been kept at a constant value of 0.1 cm throughout all the runs. Additional parameters shown in the figure are the radii R_v and R_f. R_f is the kernel radius at the beginning of interaction. R_v is the sum of the core radius of each vortex (σ) and the distance between the center line and the center of vortex (0.1 cm). Therefore, it provides a measure of the extent of the vortex pair. It is seen that the core radius does not change much during the interactions; hence, the initial value is taken to represent the vortex size throughout the simulation. The interaction begins when the center of the vortex is at distance $\sigma + R_f$ from the center of the kernel.

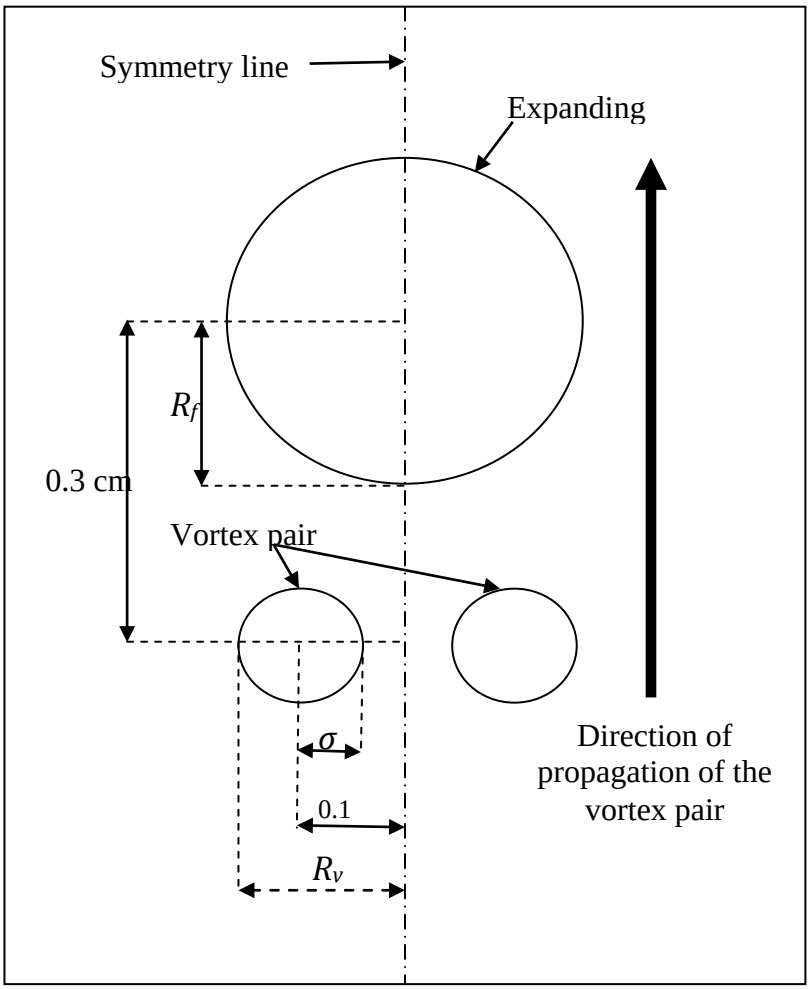

Figure 2.1: Schematic of the flame kernel-vortex computational configuration.

The conditions for the simulations are listed in Table 2.1. The vortex parameters, $u_{\theta,\max}$ and R_v, and their corresponding regime are also listed. Sixty two runs were made, which include all the various regimes of the KV interactions presented in this study. Each interaction has been placed in a specific regime depending on how the kernel reacts when it is impinged by

the vortex pair. This table forms the basis of the spectral diagram that is discussed in a later section. The computations were performed on 4 Intel Xeon™ 3.2GHz, which are part of the NC State HPC cluster. Typical computation times range from 8 to 12 hours.

Table 2.1: Run conditions.

$u_{\theta,\max}$ (cm/s)	R_v (cm)	*Regime*	$u_{\theta,\max}$ (cm/s)	R_v (cm)	*Regime*
10000	0.2	Breakthrough	21000	0.2	Global Extinction
20000	0.2	Global Extinction	12500	0.22	Breakthrough
15000	0.2	Breakthrough	14000	0.25	RGE
1000	0.2	Wrinkled kernel	14500	0.25	Breakthrough
2500	0.2	Wrinkled kernel	15000	0.25	Global Extinction
5000	0.2	Breakthrough	16000	0.25	Global Extinction
17500	0.27	Global Extinction	16000	0.3	Breakthrough
7500	0.25	Breakthrough	19000	0.2	Global Extinction
2500	0.15	Wrinkled kernel	16000	0.27	RGE
2500	0.3	Wrinkled kernel	20000	0.18	Global Extinction
5000	0.15	Breakthrough	17500	0.25	Global Extinction
10000	0.3	Breakthrough	15000	0.28	Breakthrough
200	0.2	Laminar kernel	20000	0.25	Global Extinction
200	0.15	Laminar kernel	17500	0.22	Global Extinction
17500	0.2	Global Extinction	16000	0.2	Global Extinction
17500	0.15	Breakthrough	20000	0.18	Global Extinction
12500	0.15	Breakthrough	10000	0.4	Wrinkled kernel
100	0.15	Laminar kernel	6000	0.28	Wrinkled kernel
7500	0.15	Breakthrough	15500	0.23	Global Extinction
7500	0.2	Breakthrough	13500	0.22	Breakthrough
7500	0.25	Breakthrough	17500	0.3	RGE
17500	0.3	Breakthrough	17500	0.33	RGE
12500	0.25	Breakthrough	17500	0.27	Global Extinction
10000	0.32	Breakthrough	300	0.25	Laminar kernel
17500	0.29	RGE	20000	0.33	RGE

Table 2.1: Continued

1500	0.4	RGE	1000	0.2	Wrinkled kernel
12500	0.4	Winkled kernel	13000	0.43	Wrinkled kernel
14500	0.28	RGE	14500	0.3	RGE
7500	0.33	Wrinkled kernel	13000	0.4	Breakthrough
10000	0.11	Wrinkled kernel	7500	0.11	Wrinkled kernel
200	0.22	Laminar kernel	500	0.15	Laminar kernel
500	0.2	Laminar kernel	500	0.25	Laminar kernel

Chemical rates are obtained from GRI-Mech 2.11 mechanism, developed by Frenklach et al. (1995), with carbon-containing species removed. Table 2.2 provides with the list of nineteen $H_2 - O_2$ reactions which are listed in GRI-Mech 2.11. Transport properties are based on a multi-component mixture-averaged formulation.

Table 2.2: Hydrogen-Air Mechanism. Rate constants in the form of $k = AT^{\beta}e^{(-Ea/T)}$

	Reaction	A	β	Ea (kcal/mol)
1.	$O+H_2 \Leftrightarrow H+OH$	5.00×10^4	2.67	6.29
2.	$O+H+M \Leftrightarrow OH+M$	5.00×10^{17}	-1.0	0.0
3.	$O+HO_2 \Leftrightarrow OH+O_2$	2.00×10^{13}	0.0	0.0
4.	$O+H_2O_2 \Leftrightarrow OH+HO_2$	9.63×10^6	2.0	4.0
5.	$H+O_2+M \Leftrightarrow HO_2+M$	2.8×10^{18}	-0.86	0.0
6.	$H+2O_2 \Leftrightarrow HO_2+O_2$	3.0×10^{20}	-1.72	0
7.	$H+O_2+H_2O \Leftrightarrow HO_2+H_2O$	9.38×10^{18}	-0.76	0.0
8.	$H+O_2 \Leftrightarrow O+OH$	8.3×10^{13}	0.0	14.413
9.	$2H+M \Leftrightarrow H_2+M$	1.00×10^{18}	-1.0	0.0
10.	$2H+H_2 \Leftrightarrow 2H_2$	9.00×10^{16}	-0.6	0.0
11.	$2H+H_2O \Leftrightarrow H_2+H_2O$	6.00×10^{19}	-1.25	0.0
12.	$H+OH+M \Leftrightarrow H_2O+M$	2.20×10^{22}	-2.0	0.0
13.	$H+HO_2 \Leftrightarrow O+H_2O$	3.97×10^{12}	0.0	0.671

Table 2.2: Continued

14.	$H+HO_2 \Leftrightarrow O_2+H_2$	2.8×10^{13}	0.0	1.068
15.	$H+HO_2 \Leftrightarrow 2OH$	1.34×10^{14}	0.0	0.635
16.	$H+H_2O_2 \Leftrightarrow HO_2+H_2$	1.21×10^{7}	2.0	5.2
17.	$H+H_2O_2 \Leftrightarrow OH+H_2O$	1.0×10^{13}	0.0	3.6
18.	$OH+H_2 \Leftrightarrow H+H_2O$	2.16×10^{8}	1.51	3.43
19.	$2OH \Leftrightarrow O+H_2O$	3.57×10^{4}	2.4	-2.11

CHAPTER 3

Kernel-Vortex Interaction Regime: Part I

This chapter presents a description of the different regimes that have been addressed by Echekki and Kolera (2007). The different KV interactions have been grouped into four distinct regimes characterized by the extent to which the dynamics and structure of the kernel are impacted by its interaction with the vortex pair. These regimes include the ones previously discussed by Echekki and Kolera-Gokula (2007). Namely, these regimes are, 1) the laminar kernel regime, 2) the wrinkled kernel regime, 3) the breakthrough regime, and 4) the global extinction regime.

3.1 The laminar kernel regime

This regime corresponds to KV interactions when a small and weak vortex pair impinges on the expanding kernel. Vortices dissipate very quickly due to the high viscosity region present around the kernel due to the presence of high-temperature products. The extent of deformation caused by the vortices is very small, and they are unable to induce significant stretch on the kernel. In order to have distinction between laminar kernel and wrinkled kernel regime, a penetration parameter 'd' is used. If $d/R_v < 5$, then the interaction is characterized as a laminar kernel interaction.

Figure 3.1 shows the evolution of the H_2 consumption rate contours at different times of the KV interaction in the laminar kernel regime for R_v = 0.15 cm and $u_{\theta,\max}$ = 100 cm/s. To

provide comparison of the present results in the laminar kernel regime to other results in the remaining 4 regimes, the same scale is adopted to plot the H_2 consumption rate contours. Moreover, only a small window of the computational domain is shown in this figure and subsequent figures, which corresponds to a lateral extent of 1.4 cm and a longitudinal extent (along the vortex displacement direction) of 1.4 cm. The interaction begins at 0.119 ms, which is relatively delayed in comparison of the KV interactions associated with other regimes, which are discussed below. This delay is due to the small vortex size and its slow translation velocity. As seen at 0.456 ms, effects of the vortex pair can be seen on the expanding kernel. Initially, the flow field of the vortex flattens the flame and as time progresses, it causes a small amount of wrinkling of the kernel. After 1.116 ms, the vortex core starts to dissipate due to the high viscosity and high temperature near the flame. The figure also shows that with the exception of the early kernel rate of consumption, which is enhanced by both the initial heating for ignition and its strong curvature, the overall structure of the flame appears to be unchanged along the flame kernel surface and at different times of the interactions. The flame kernel in the laminar kernel regime is not affected by the imposed strain of the vortex pair or the overall evolution of the global stretch rate of the expanding kernel.

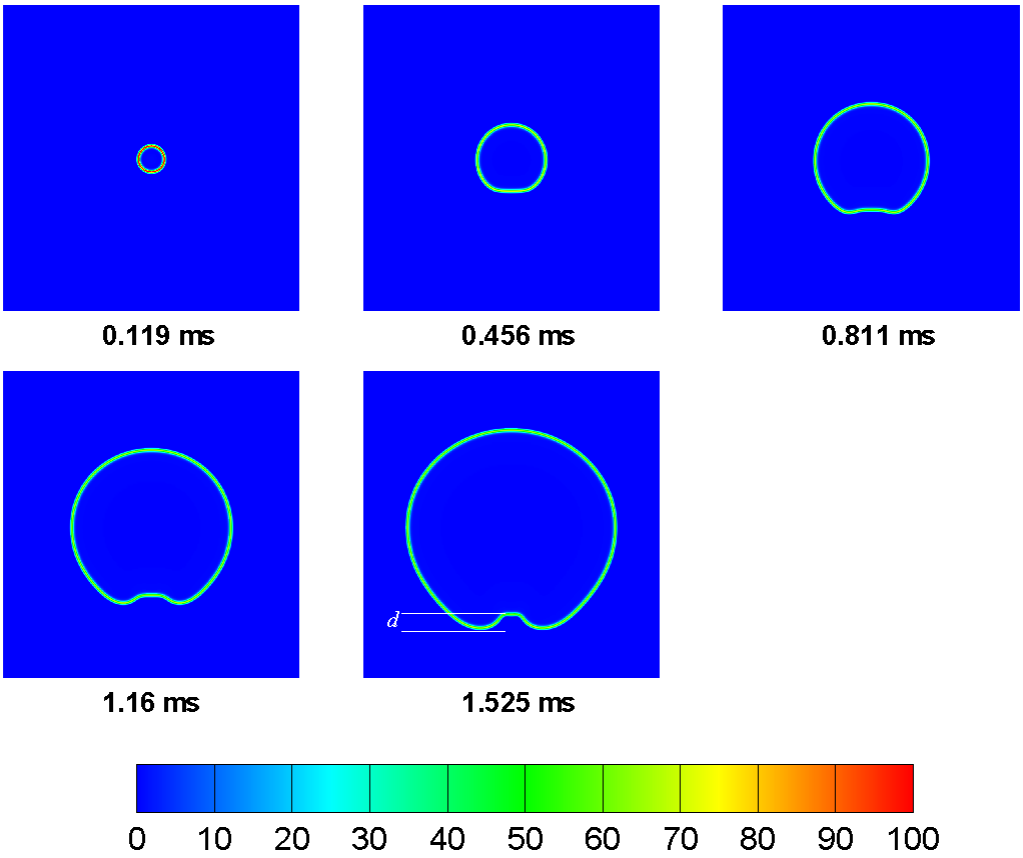

Figure 3.1: Transient snapshots of interaction of kernel with vortex pair with R_v = 0.15 cm and $u_{\theta,max}$ = 100 cm/s. The contours depict the H_2 consumption rate.

Another example of the laminar kernel is shown in figure 3.2. Effect of the vortex can be seen at 0.407 ms as the expanding kernel is flattened. Under the influence of the vortex pair, the expanding kernel is further distorted and a notch is developed as seen at 1.44 ms. Vortex pair starts to dissipate and after 1.61 ms the stretch induced by the vortices has no effect on the expanding kernel. The vortex parameters in these interactions are R_v = 0.2 cm and $u_{\theta,max}$ = 200 cm/s.

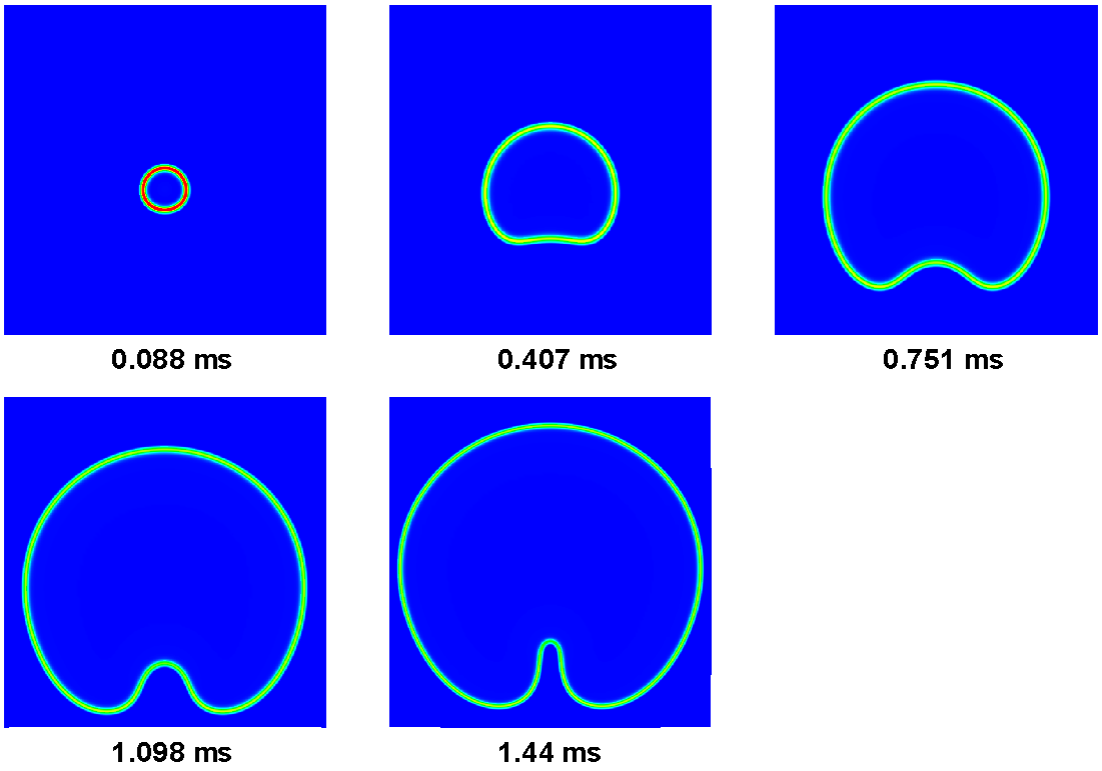

Figure 3.2: Transient snapshots of interaction of kernel with vortex pair with R_v = 0.2 cm and $u_{\theta,max}$ = 200 cm/s. The contours depict the H_2 consumption rate.

3.2 The wrinkled kernel regime

The wrinkled kernel regime is characterized by KV interactions when vortices are strong enough to cause significant deformation of the expanding kernel, but are unable to punch through it. Flame surface deformation is the sole criterion that governs the transition of interactions from laminar kernel to wrinkled kernel regime. As the vortex pair penetrates the kernel, a notch is formed on the trailing edge of the flame. When the vortex dissipates, the flame kernel continues to grow and "pushes" against the vortex pair due the expansion of the burned gases within the kernel.

Figure 3.3 shows contours of the H_2 consumption rate for R_v = 0.25 cm and $u_{\theta,\max}$ = 4000 cm/s. Again, the same contour scale is used here as in Fig. 3.1. Unlike the laminar kernel regime, the effect of the vortices on the expanding kernel can be seen at a much earlier time as seen at 0.024 ms. At the beginning of interaction, the kernel is flattened on the trailing edge. Due to the higher translation velocity, the vortex penetrates deeper in to the expanding kernel as seen at 0.212 ms. The vortex carries the trailing edge of the flame along with it until it reaches the leading edge, and downstream flame-flame interactions occurs. These interactions can be seen from 0.421 ms onwards. By this time, the vortex core is surrounded by hot gases on all sides and engulfed by the kernel. Finally, the vortices are completely dissipated by the hot products and the edges of the kernel fuse together. As seen at 1.1 ms the kernel continues to grow further and the notch resulting from the penetration of the vortex is blunted by the expanding kernel.

The kernel structure is also affected by the straining and wrinkling effects of the vortex pair. At 0.212 and 0.421 ms, regions of enhanced H_2 consumption are associated primarily with downstream flame-flame interactions. Both this enhanced consumption rate and the more intense wrinkling of the kernel by the vortex pair results in faster rates of growth of the kernel relative to comparable times in Fig. 3.1. At subsequent stages of the interactions after the vortex pair strength is dissipated, the overall rates of H_2 consumption are similar to those observed in Fig. 3.1 in the laminar kernel regime.

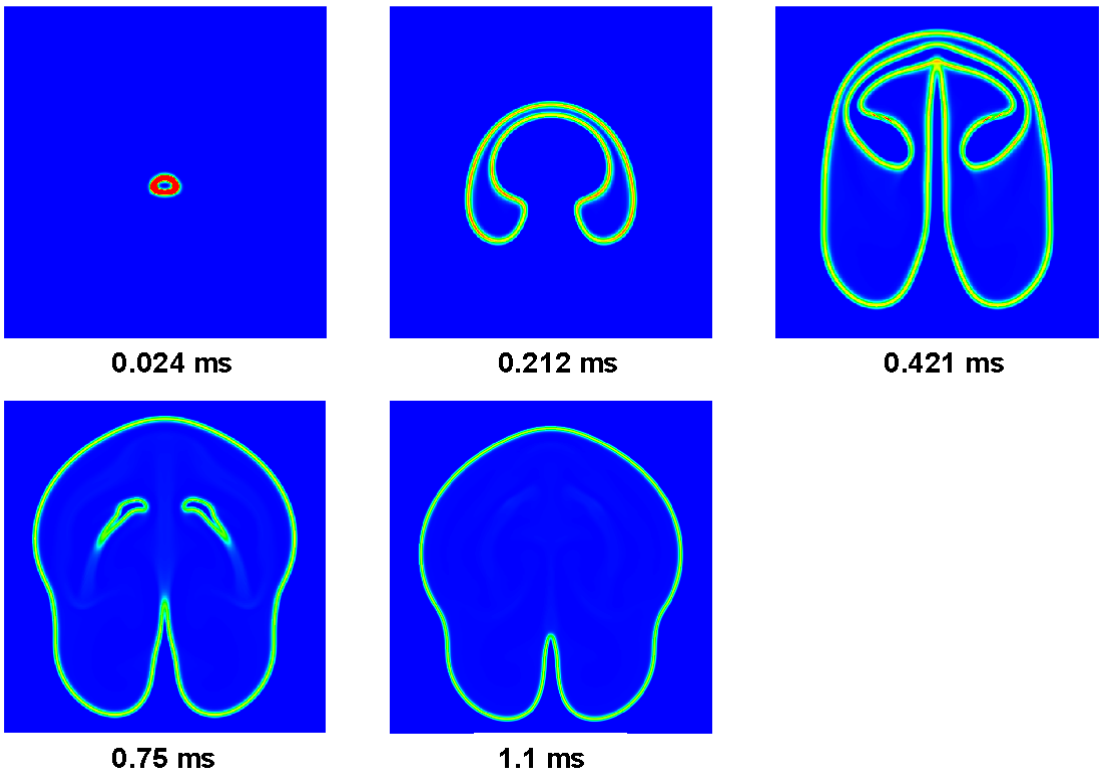

Figure 3.3: Transient snapshots of interaction of kernel with vortex pair with R_v = 0.25 cm and $u_{\theta,max}$ = 4000 cm/s. The contours depict the H_2 consumption rate.

Figure 3.4 shows transient snapshots of another interaction in the same regime. The vortex parameters in this case are R_v = 0.28 cm and $u_{\theta,\max}$ = 6000 cm/s. Vortex pair is impinged on the kernel at 0.018 ms which is visible as the kernel is flattened. At 0.227 ms, the kernel begins to engulf the vortex. Due to the high strain induced by the large vortex pair on the kernel, at 0.476 ms, the leading edge of the flame is about to get extinguished locally. At 0.539 ms, the vortex pair is dissipated in the kernel, after which the kernel grows and expands till it fills the entire domain. This interaction is at the border of the wrinkled kernel and breakthrough regime. This can be said because, the leading edge of the kernel begins to open but, as the vortex is dissipated, it is unable to punch through the kernel.

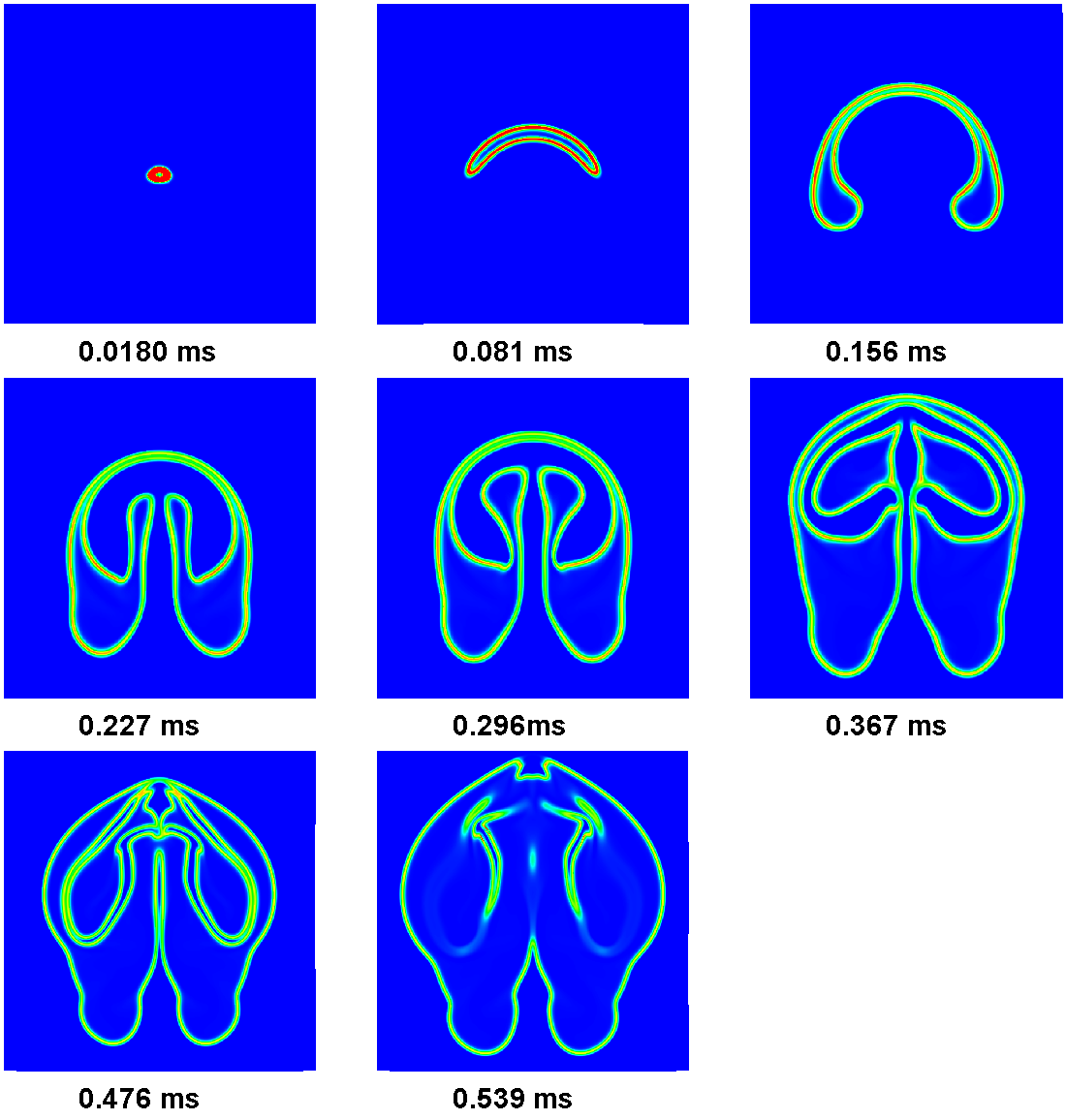

Figure 3.4: Transient snapshots of interaction of kernel with vortex pair with R_v = 0.28 cm and $u_{\theta,\max}$ = 6000 cm/s. The contours depict the H_2 consumption rate.

3.3 The breakthrough regime

In the breakthrough regime, the vortices are strong enough to travel through the kernel without getting dissipated. This results in the splitting of the flame kernel into two kernels, which may eventually fuse to form a new single deformed kernel. Figure 3.5 shows the H_2 consumption rate contours for conditions in the breakthrough regime with R_v = 0.15 cm and $u_{\theta,\max}$ = 17500 cm/s. As seen at 0.0467 ms, the leading and the trailing edges of the flame are fused together and mutual annihilation can be seen at 0.0825 ms. As a consequence of this, the leading edge of the flame is extinguished. The vortex pair causes the kernel to split into two flame kernels, as seen at 0.118 ms. The vortex is still strong enough to cause further wrinkling of the parallel edges of the flames. Eventually the vortex translates downstream and is ejected from the kernel and the two flames recombine and grow as seen at 0.198 ms.

Again, the more prevalent presence of downstream flame-flame interactions results in significant enhancements in the H_2 consumption rate. The same process is responsible for the mutual extinction of the interacting flame elements as observed between 0.0467 and 0.0825 ms after fusion of the leading and trailing edges of the kernel. Ranganath et al. (2005) and Kolera-Gokula et al. (2007) showed that, the flame-flame interactions in hydrogen flames involve important interplays between diffusive transport and chemistry resulting from the different rates of diffusion of the fuel and the oxidizer.

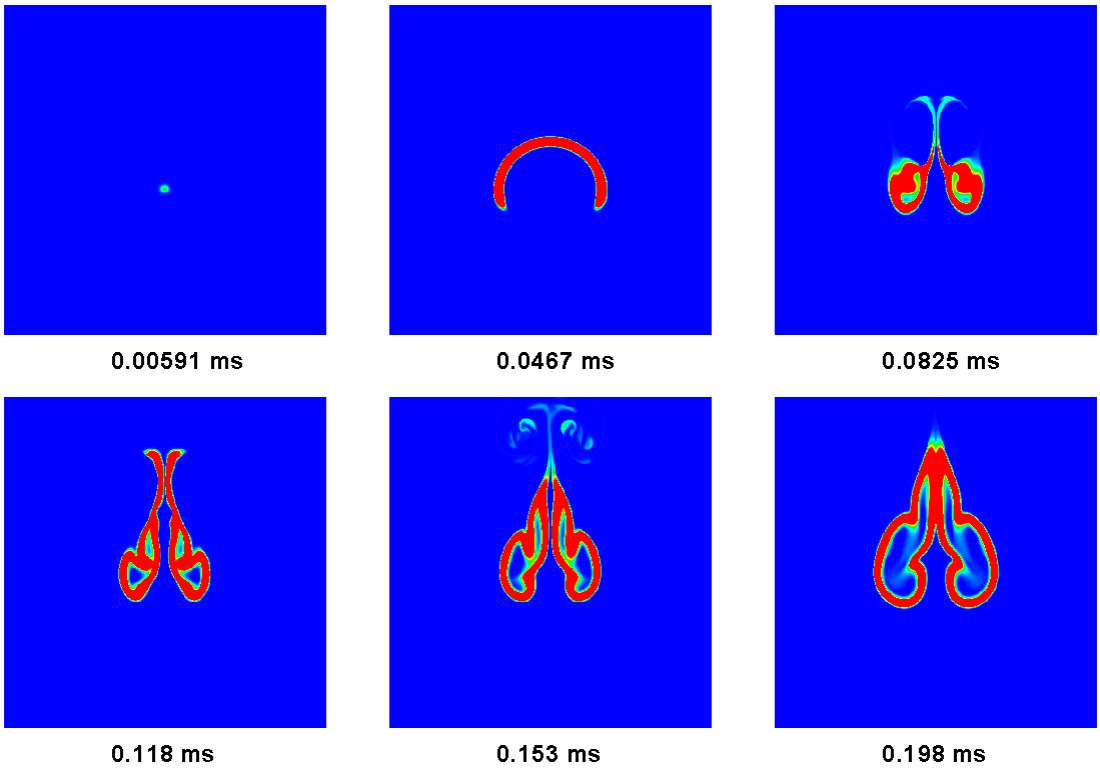

Figure 3.5: Transient snapshots of interaction of kernel with vortex pair with R_v = 0.15 cm and $u_{\theta,\max}$ = 17500 cm/s. The contours depict the H_2 consumption rate.

Figure 3.6 shows another interaction in this regime with the vortex having parameters R_v = 0.25 cm and u_θ = 14500 cm/s. As compared to the previous case, the vortex strength is slightly less but the vortex size is much large. Consequently, the hydrodynamic strain imposed on the kernel is higher. The vortex pair pushes the trailing edge until it meets the leading edge, and due to flame-flame interactions there is mutual annihilation. Due to the high penetration power of the vortex, it punches through the kernel dividing it into two flames as seen at 0.0895 ms

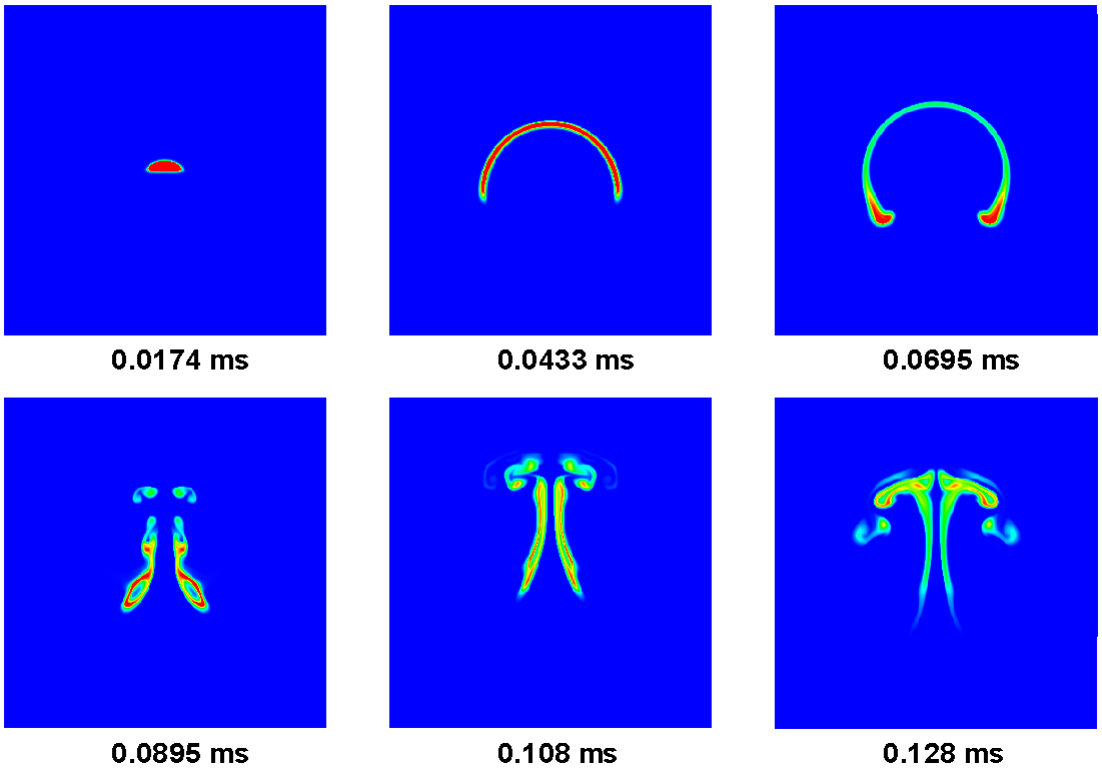

Figure 3.6: Transient snapshots of interaction of kernel with vortex pair with R_v = 0.25 cm and $u_{\theta,\max}$ = 14500 cm/s. The contours depict the H_2 consumption rate.

3.4 The global extinction regime

The global extinction regime is characterized by large and strong vortices. As the vortex pair interacts with the expanding kernel, large stretch and strain is induced on the kernel. As a result, the kernel has “no room” to expand, and eventually extinguishes under the intense hydrodynamic stretch imposed by the vortex pair. Figure 3.7 shows H_2 consumption rate contours for R_v = 0.25 cm and $u_{\theta,\max}$ = 17500 cm/s. The vortex causes the kernel to fuse as the leading and trailing edges are pushed into each other as seen at 0.0469 ms. As seen at 0.0756 ms, vortex causes high stretch on the kernel and the flame breaks into smaller flamelets which later extinguish at 0.1805 ms.

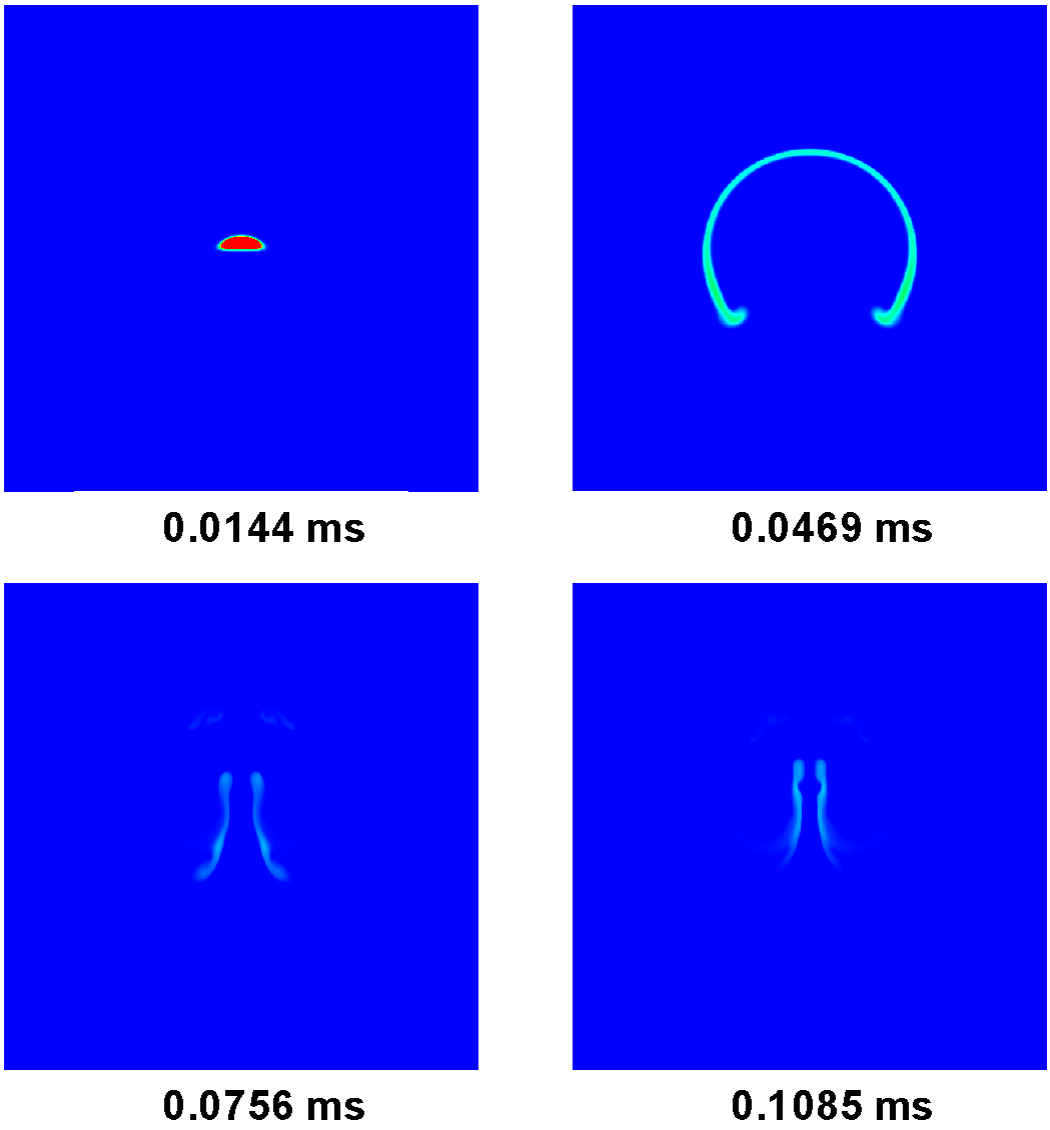

Figure 3.7: Transient snapshots of interaction of kernel with vortex pair with R_v = 0.25 cm and $u_{\theta,\max}$ = 17500 cm/s. The contours depict the H_2 consumption rate.

Figure 3.8 shows another interaction in the same regime with the vortex having parameters R_v = 0.3 cm and u_θ = 20000 cm/s. As compared to previous example, a stronger and a larger vortex pair is interacting with the kernel. Due to the high translation velocity and large size of the vortex, the kernel feels the effect of the vortex at realtively early time of 0.0059 ms as compared to the case in figure 3.7. This causes a flattening of the kernel. Due to very high stretch induced by the vortex, the kernel is extinguished at 0.0933 ms.

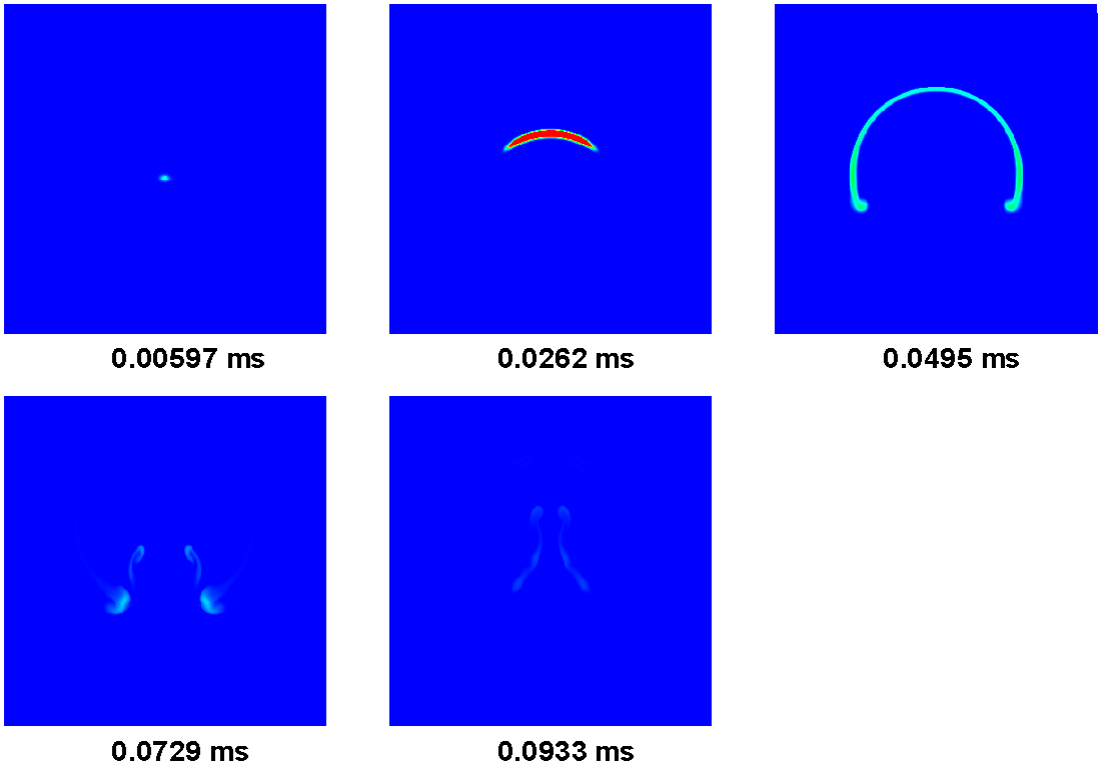

Figure 3.8: Transient snapshots of interaction of kernel with vortex pair with R_v = 0.3 cm and $u_{\theta,\max}$ = 20000 cm/s. The contours depict the H_2 consumption rate.

CHAPTER 4

Kernel-Vortex Interaction Regime: Part II

This chapter discusses a new, fifth, regime that is observed, which corresponds to the regeneration-after-global-extinction (RGE) regime. The sections below discuss this regime and attempt to identify any pertinent role chemistry plays during the interactions. A case in which lean mixture (equivalence ratio = 0.5) proportion was used for the interaction, which generated RGE regime, is also presented.

4.1 Regeneration after global extinction regime

The RGE regime has not been observed in previous experimental and computational studies, and is illustrated here in this study. KV interactions in this regime proceed initially in a manner similar to global extinction; but, the interactions are followed by a regeneration process and a resumption of combustion. Important multi-step chemical kinetic effects coupled with transport are expected to play an important role in this regime. In this regime, the vortices are strong and large (relative to the kernel) as in the global extinction regime. These vortices almost entirely extinguish the flame except at the trailing edge of the flame. These edges are not only contorted by the strong vortices but, they are also fed with reactants from all the sides. Consequently, these flames survive and grow and evolve into complex flame structures and topologies assisted by further flame-generated vorticity.

Figure 4.1 shows H_2 consumption rate contours in the RGE regime corresponding to R_v = 0.3 cm and $u_{\theta,\max}$ = 17500 cm/s. These parameters place the operation within this regime at relatively high-speed conditions and at ratios of $u_{\theta,\max}/S_L$ above 130. The leading and trailing edges of the flame kernel are fused at 0.0566 ms. Due to the high stretch imposed on the flame by the large vortex, the bulk of the kernel is extinguished by the resulting downstream flame interactions, except for its edges, which are broken into segments as seen at 0.0932 ms. The resulting segments have no distinct flamelet structures as observed in the laminar kernel or wrinkled kernel regime. Instead, the reacting segments correspond to a collection of fused reaction hot spots resulting in overall broadening of the reaction region (see for example the H_2 consumption rate contours at 0.228 and 0.27 ms). While some segments are extinguished, as shown between 0.152 ms and 0.19 ms, others are reignited in a continuous interplay between stretching and flame-flame interactions effects countered by reignition and the mending of reaction segments. Moreover, the reaction intensity at the combustion hot spots is similar in magnitude to the conditions encountered in the earlier regimes, as these spots remain surrounded by fresh reactants. We speculate that the re-ignition process is enabled by the supply of hot products providing both heat and radical species and fresh reactants.

The vorticity contours shown in Fig. 4.1 also illustrate the complex role of the interaction of the kernel and the vortex that results in both the “shredding” of the flame kernel and the generation of vorticity due to the complex interactions of the vortex pair with different layers of flame segments. It is these secondary vortices (not the original vortex pair) that appear to sustain the combustion process after the passage of the original vortex pair.

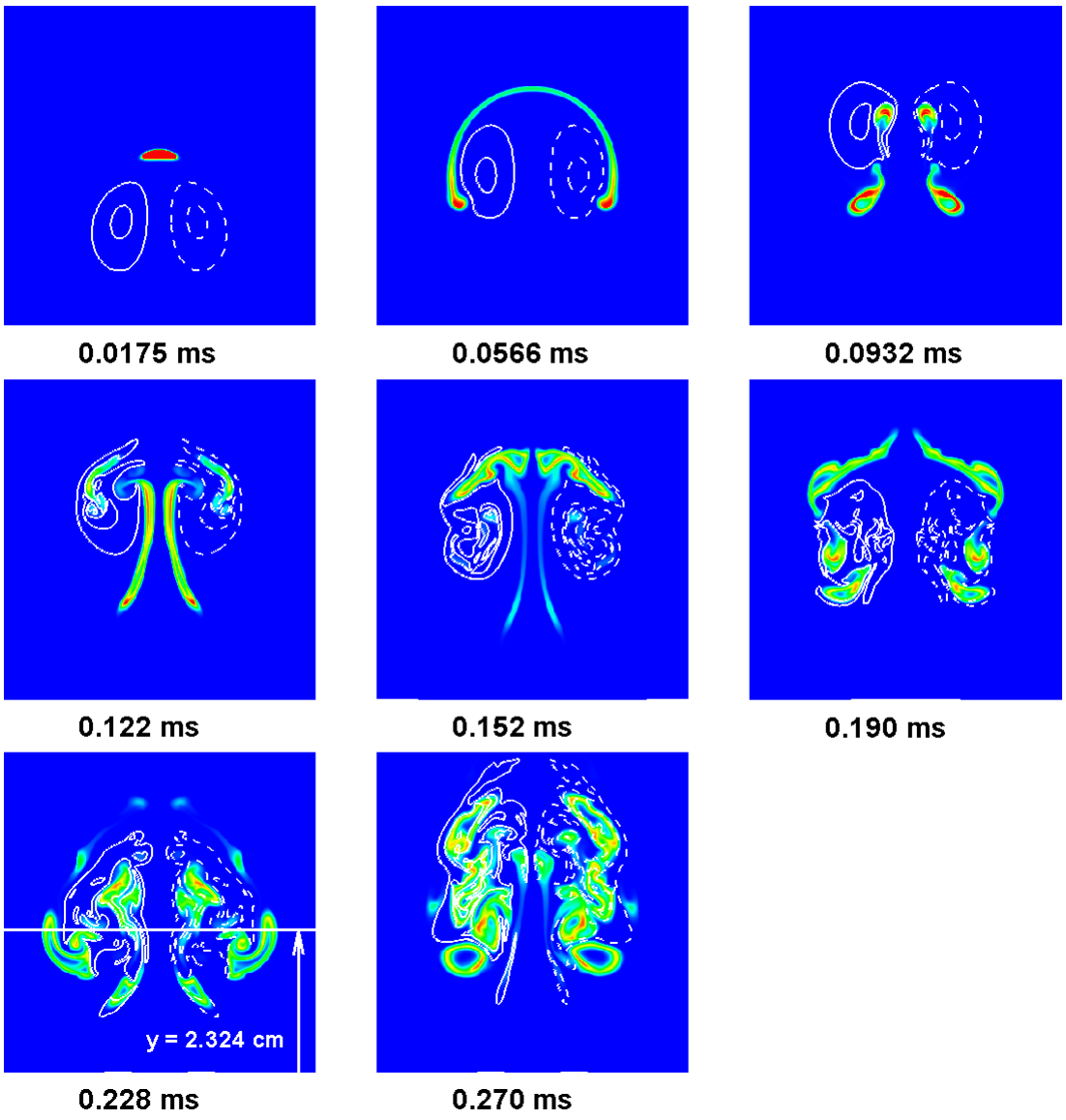

Figure 4.1: Transient snapshots of interaction of kernel with vortex pair with R_v = 0.3 cm and $u_{\theta,\max}$ = 17500 cm/s. The contours depict the H_2 consumption rate. Solid white lines: negative vorticity; dashed white lines: positive vorticity.

Figure 4.2 shows 1D cuts of the H_2 consumption rate and temperature profiles (at 0.228 ms) across the spanwise direction (y = 2.324 cm from origin) of the vortex displacement (as shown in Fig. 4.1) corresponding to R_v = 0.3 cm and $u_{\theta,\max}$ = 17500 cm/s. H_2 consumption, as expected, is interpreted as a marker of chemical activity; while, temperature is interpreted as a marker of completion of the combustion process (i.e. a reaction progress variable). The profiles show the presence of more than a single peak of the hydrogen consumption rate and the temperature illustrating the complex nature of the reaction zone structure. With the exception of one peak, all H_2 consumption rate and temperature peaks coincide indicating an active combustion zone. In the one exception, the reaction is decaying as the combustion process is completed, consistent, with the standard premixed flame structure. Mole fractions of reactants (H_2 and O_2) and products (H_2O) are also subsequently shown in figure 4.3. The mole fraction profiles reflect the observations made based on Fig. 4.2. An additional noteworthy observation is that, sharp gradients of H_2 mole fractions are greatly smoothed due to H_2's higher mass diffusion relative to the oxidizer and the product, H_2O. Therefore, non-even profiles equivalence ratios are expected within the reaction region.

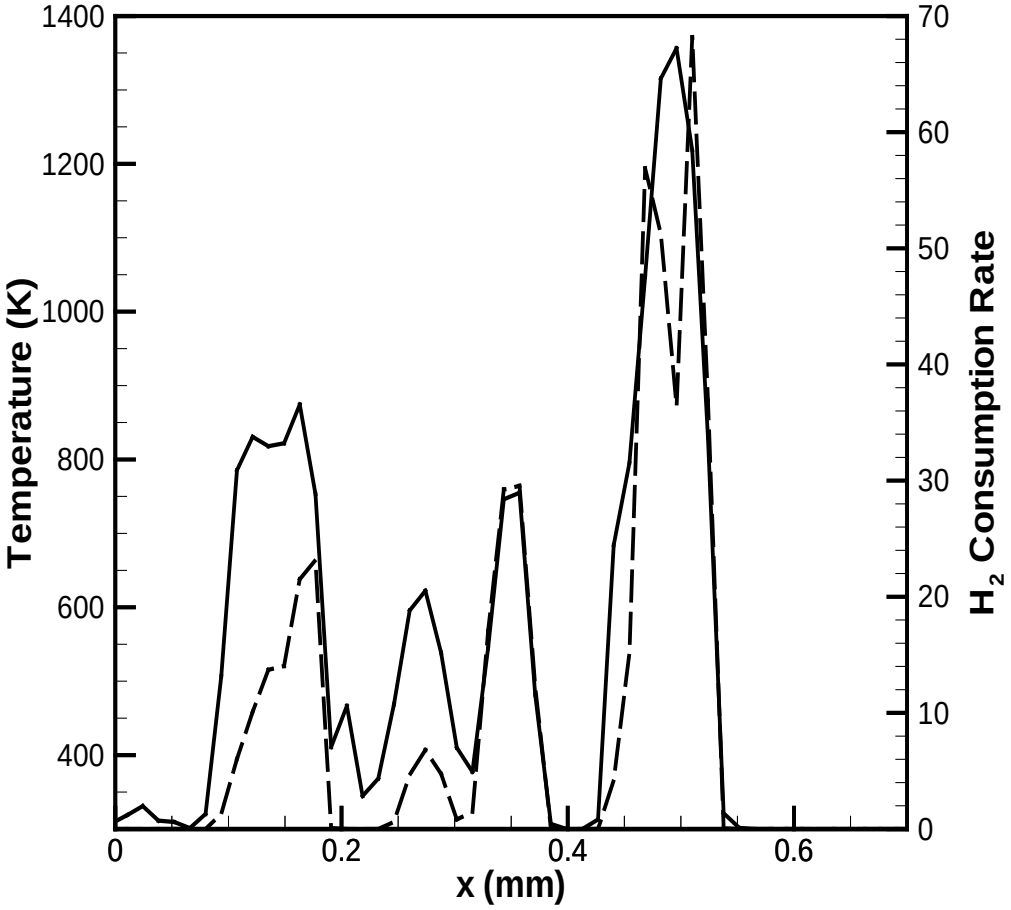

Figure 4.2: H_2 Consumption rate and temperature vs. spanwise length of flame. Symbols: ——: Temperature; - - - - - : H_2 consumption rate.

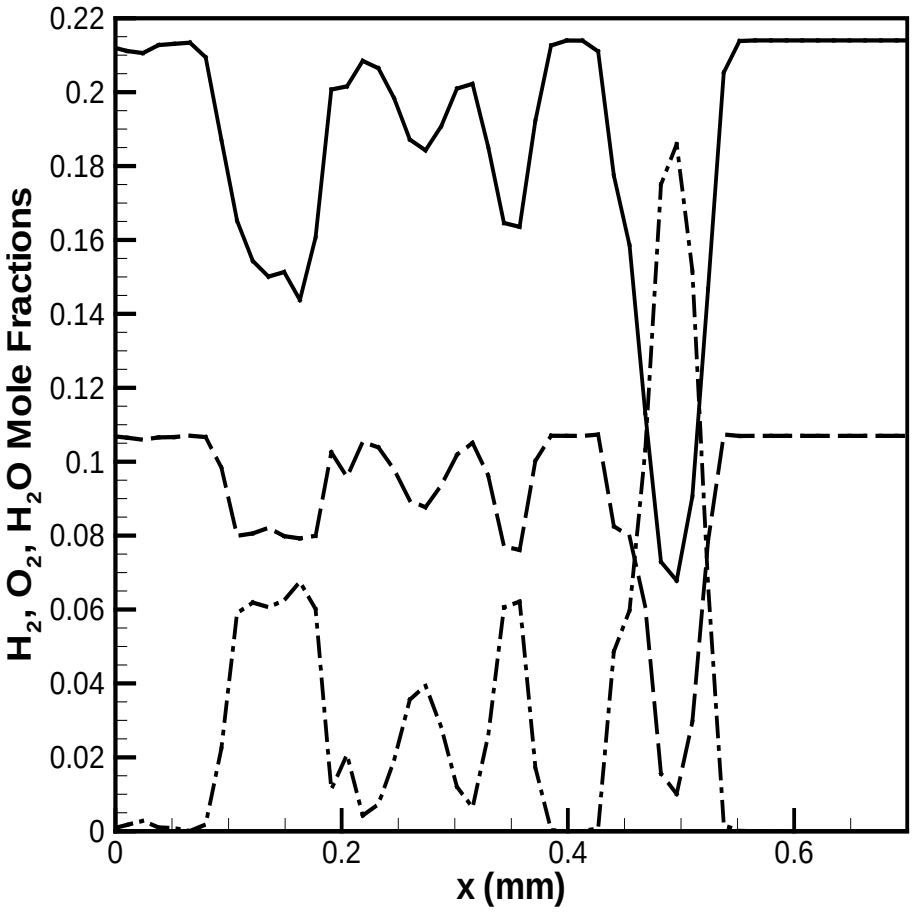

Figure 4.3: H_2, O_2, H_2O Mole fractions vs. spanwise length of flame. Symbols: ——— : H_2 mole fraction; - - - - - : O_2 mole fraction; - · - · - · - : H_2O mole fraction.

Figure 4.4 shows another interaction in the RGE regime, with smaller vortex pair, R_v = 0.27 cm, and a lower strength, $u_{\theta,\max}$ = 1600 cm/s, as compared to the previous case. As seen from Fig. 4.4, the vortex pair breaks the kernel into different “flame” segments at 0.0885 ms. Similar to the previous discussion, the vortex extinguishes the bulk of the kernel, but the remaining “flame” segments continue to stretch and grow as shown for times, 0.182 ms onwards.

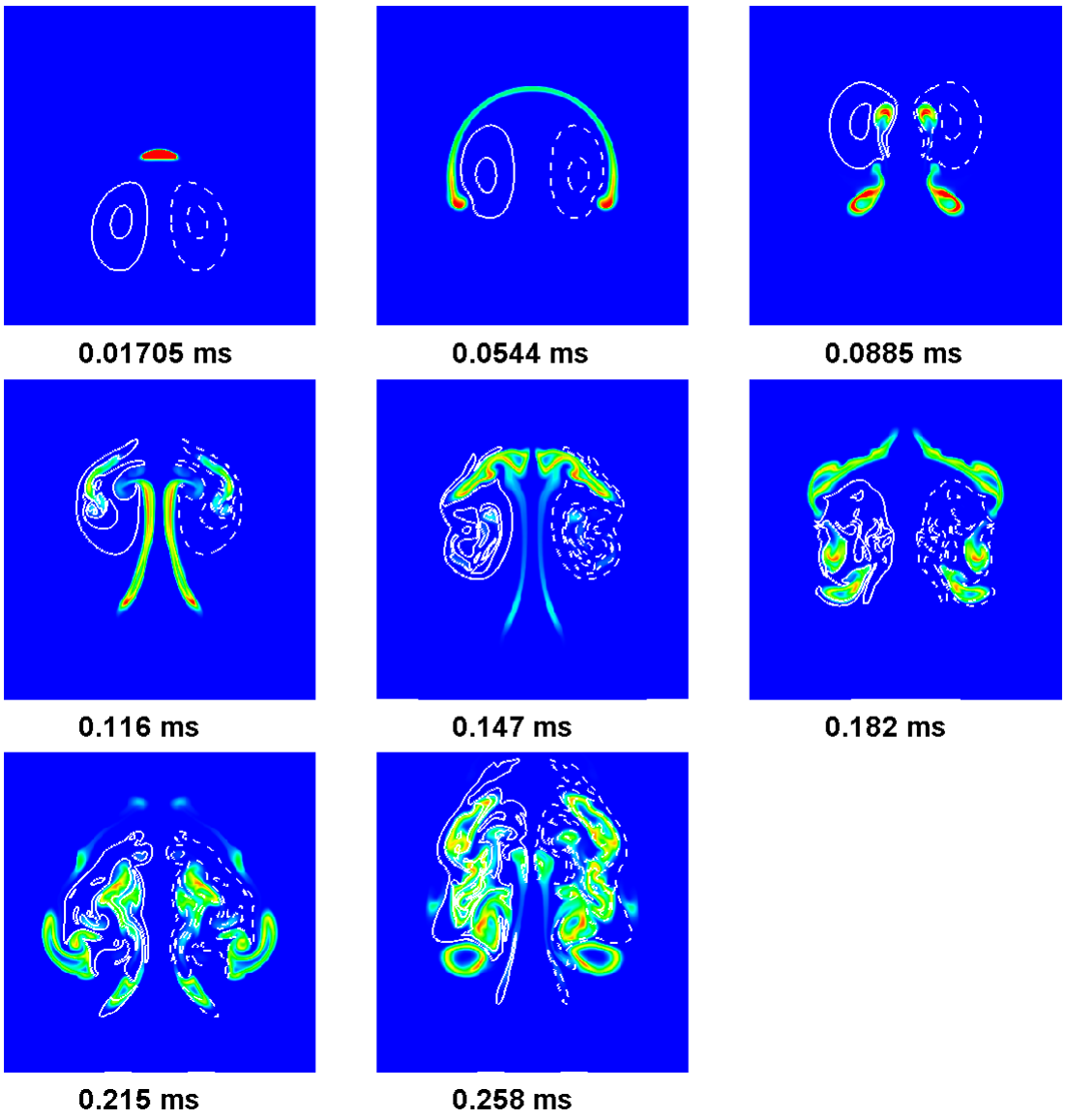

Figure 4.4: Transient snapshots of interaction of kernel with vortex pair with R_v = 0.27 cm and $u_{\theta,\max}$ = 16000 cm/s. The contours depict the H_2 consumption rate. Solid white lines: negative vorticity; dashed white lines: positive vorticity.

4.2 The RGE regime with a lean mixture

Another display of regeneration within the RGE regime is illustrated with a much leaner mixture corresponding to an equivalence ratio of 0.5. Figure 4.5 shows the evolution of the H_2 consumption rate in the RGE regime for R_v = 0.25 and $u_{\theta,\max}$ = 17500. The same vorticity parameters resulted in global extinction for the stoichiometric conditions (see Figure 3.7). The reduced equivalence ratio also results in a significantly lower reference flame speed, S_L and a higher ratio, $u_{\theta,\max}/S_L$. Moreover, the kernel at leaner conditions is subject to an increased potential for the onset of thermo-diffusive instabilities. The regeneration process, as in the stoichiometric case, proceeds through an initial step of global extinction. However, for the RGE case, the edges of the kernel remain ignited. At 0.226 ms and later, only two nascent kernels remain viable and continue to grow with the potential of seeing a similar fate to the parent kernel. The trends observed for the lean flame (Fig. 4.5) relative to the corresponding stoichiometric flame (Fig. 3.7) may appear to counter the expected trend of increasing extinction as the ratio, $u_{\theta,\max}/S_L$, in increased. In fact, by observing H_2 consumption rate contours at 0.1258 ms, it appears that global extinction was inevitable. Yet, the enhanced vorticity (relative to the case of the hotter and faster stoichiometric flame) provided enough circulation to replenish the two nascent kernels with fresh reactants.

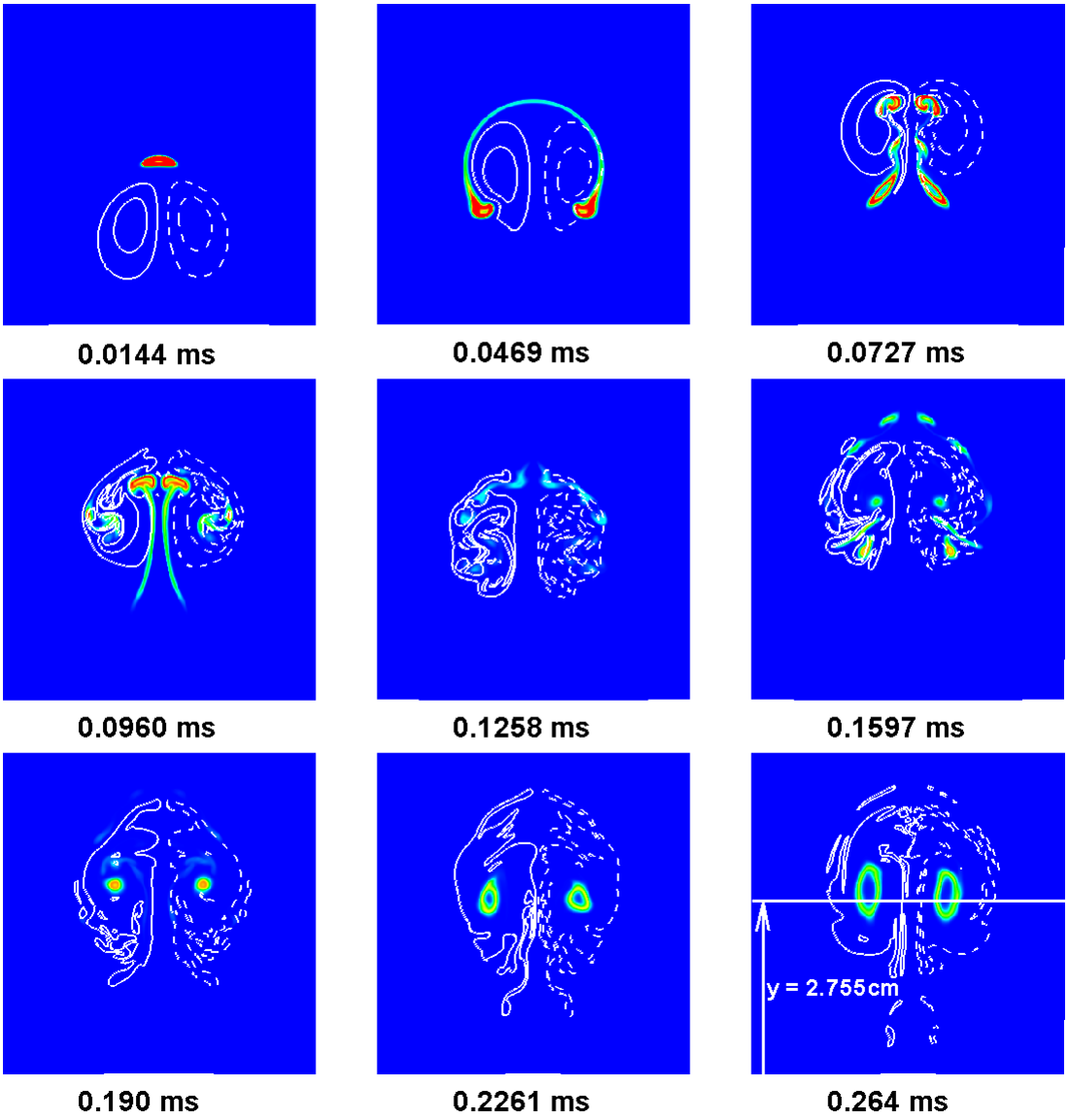

Figure 4.5: Transient snapshots of interaction of kernel with vortex pair with R_v = 0.25 cm and $u_{\theta,\max}$ = 17500 cm/s with ϕ = 0.5. The contours depict the H_2 consumption rate. Solid white lines: negative vorticity; dashed white lines: positive vorticity.

Figure 4.6 shows 1D cuts of the H_2 consumption rate and temperature profiles (at 0.264 ms) across the spanwise direction (y = 2.755 cm from origin) of the vortex displacement (as shown in Fig. 4.5) corresponding to R_v = 0.25 cm and $u_{\theta,\max}$ = 17500 cm/s. Another combustion mode in the RGE regime can be seen in the last three snapshots of figure 4.5. This mode represents a classical layered flame structure where the two kernels are formed and both of them are self sustaining. H_2 consumption, as expected, is high on the two edges of the ring of the flame (refer figure 4.6). This can be interpreted as a marker of chemical activity; while, temperature is seen to be high where the combustion process has been completed. The profiles (similar to figure 4.2) show the presence of more than a single peak of the hydrogen consumption rate. All H_2 consumption rate and temperature peaks coincide with the snapshot in figure 4.5 at 0.264 ms, indicating an active combustion zone. Mole fractions of reactants (H_2 and O_2) and products (H_2O) are also subsequently shown in figure 4.7. The mole fraction profiles reflect the observations made based on Fig. 4.6 The sharp gradients of H_2 mole fractions are greatly smoothed. This is due to H_2's higher mass diffusion relative to the oxidizer and the product, H_2O. Therefore, non-even profiles equivalence ratios are expected within the reaction region.

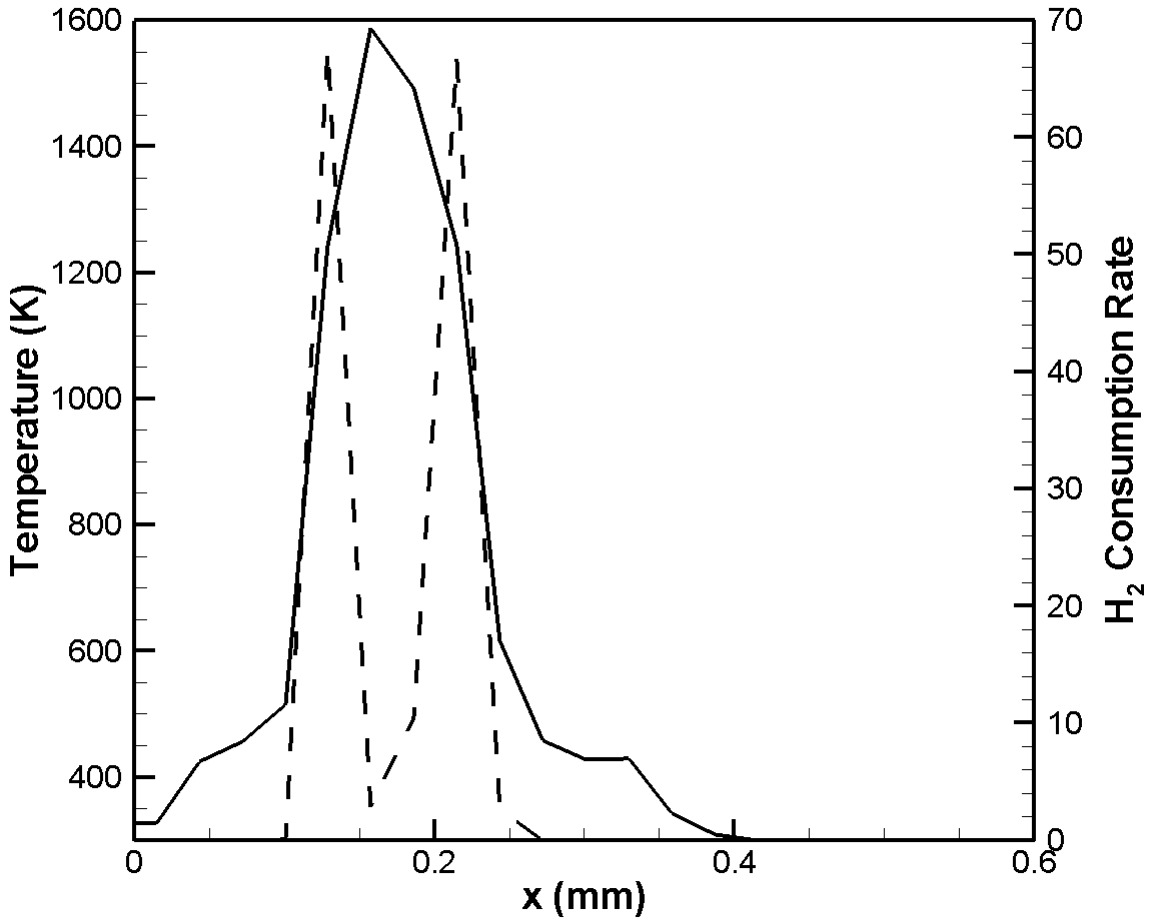

Figure 4.6: H_2 Consumption rate and temperature vs. spanwise length of flame. Symbols: ——: Temperature; - - - - - : H_2 consumption rate.

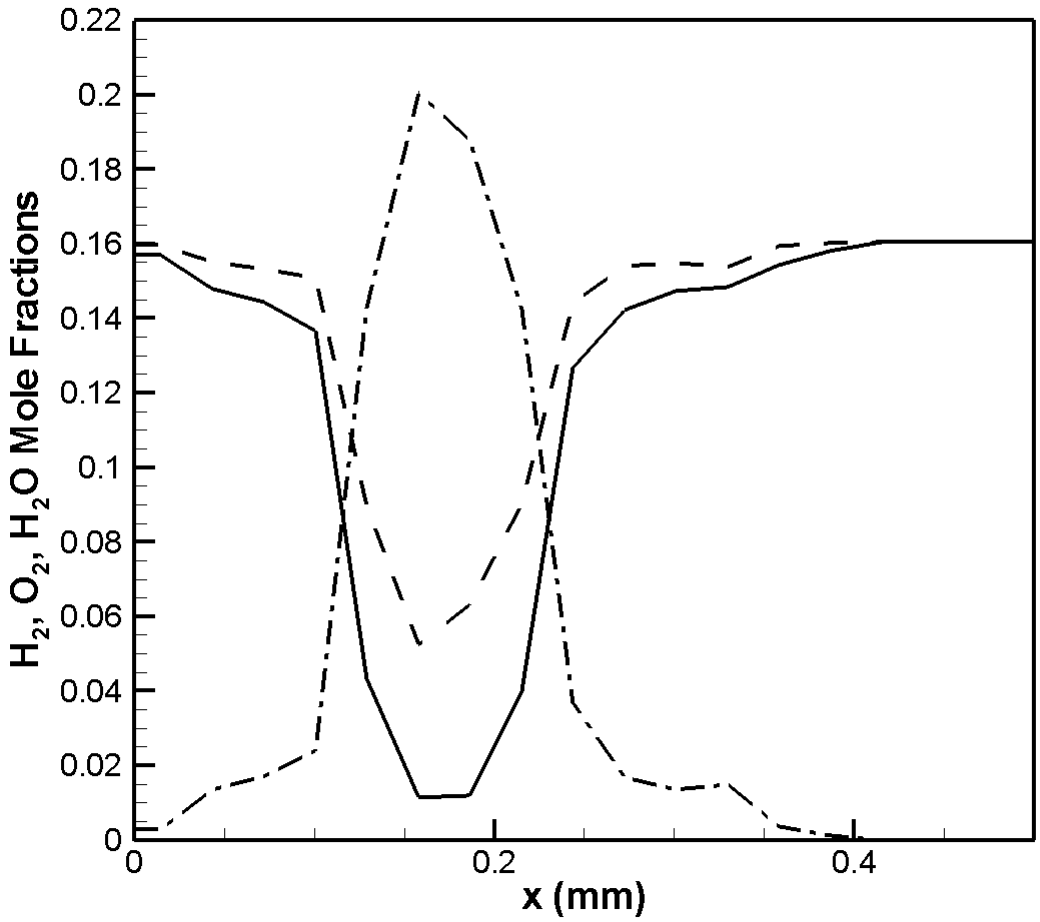

Figure 4.7: H_2, O_2, H_2O Mole fractions vs. spanwise length of flame. Symbols: ——— : H_2 mole fraction; - - - - - : O_2 mole fraction; - · - · - · - : H_2O mole fraction.

CHAPTER 5

A Revised Regime Diagram

This chapter presents the revised regime diagram, which has all-the five combustion regime present in it. The regime diagram by Echekki and Kolera-Gokula (2007) is discussed briefly, which is followed by the revised regime diagram.

5.1 Regime diagram

Recent work by Echekki and Kolera-Gokula [6] presents the interaction of a laminar flame kernel with an isolated vortex pair. The vortices are of different radii and of different strengths. Characteristic scales used to develop this spectral diagram are the relative measure of the tangential velocity of the vortex, u_θ, to the flame speed, S_L, and the ratio of the vortex size (R_v) to the size of the kernel (R_f). Previous studies by Borghi (1985) and Abdel-Gayed et al. (1989), which use the flame-vortex configuration, incorporate the length scale by considering the relative size of the vortex, R_v, to the flame thickness, δ_f. In order to take into account the unsteady mean curvature of the expanding kernel, kernel-vortex configuration, entails the usage of size of the expanding kernel, R_f, at the time of the onset of interactions. Figure 5.1 shows the regime diagram developed by Echekki et al. (2007). A two-step global reaction model for methane-air mixture was used to study the interactions.

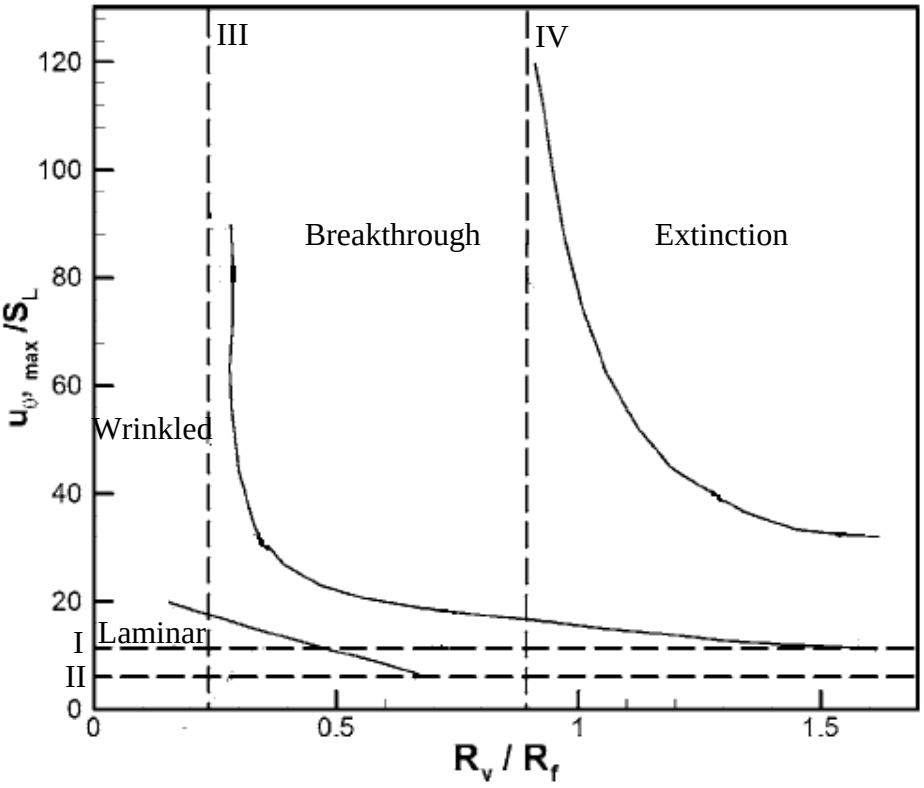

Figure 5.1: Kernel-vortex diagram from Echekki and Kolera-Gokula (2007). Data points have been removed and only boundaries have been shown.

This diagram demarcates boundaries between the laminar (no-effect) regime, wrinkled kernel (significant straining of the kernel) regime, breakthrough (extinction of the leading edge of the kernel) regime, and global extinction (total annihilation of the kernel) regime. Also, a series of limit lines have been suggested related to the ratios R_v/R_f and $u_{\theta,\max}/S_L$. These lines are:

- **I** ($(u_{\theta,\max}/S_L)\times(\rho_b/\rho_u)\approx 1$)**:** Defines the boundary of little or no impact of the vortices on the kernel (laminar kernel limit).
- **II** ($(u_{\theta,\max}/S_L)\times(\rho_b/\rho_u)\approx 2$): Defines the boundary of high straining of the kernel, but inability of the vortices to punch through the kernel (wrinkled kernel limit).
- **III** ($R_v/R_f << 1$): Defines lower boundary of breakthrough regime. Below this limit, vortices are small and they dissipate before punching through the vortex.
- **IV** ($R_v/R_f \approx 1$): Limit between breakthrough and global extinction regime.

5.2 A revised spectral diagram for KV interaction regime

Chapter 3 discusses the characteristic of the different regimes of combustion observed during KV interactions. We have indicated that we observed a new regime, which has not been listed before. It has been discussed in detail in chapter 4. The RGE regime is characterized by a number of key features with important implications to conditions of highly intense turbulence conditions.

- The RGE regime is characterized by intermittent extinction and mending/reignition processes that sustain the rate of combustion long after the primary vortex pair has passed.
- The mechanism of this regeneration process is governed by the production of combustion-generated vorticity. This vorticity appears to play a crucial role in both extinguishing and mending/reigniting “flame segments”.

- Two modes of combustion are observed within the RGE regime. The first corresponds to a well-defined flame as shown in the last 3 snapshots of H_2 consumption rate in Fig. 4.5 The second corresponds to the absence of a classical layered flame structure, which can be observed in Fig. 4.1 and Fig. 4.4. The transition between these two modes appears to be triggered by intense wrinkling from the imposed vortex structure, which promotes significant upstream and downstream flame-flame interactions. These interactions transition into an ephemeral combustion mode where fuel continues to be consumed in the absence of an identifiable layered flame structure. However, the heat released into the fluid during this phase is sufficient to reignite a new flame when the flow conditions are once again favorable to support such a structure. This flameless mode of combustion might be similar to the processes expected in the so-called distributed regime of turbulent combustion.

- It is also evident that in the RGE regime, some degree of flame shredding occurs resulting from locally intense straining and flame-flame interactions at sections of the flame. Flame shredding has been observed by Ratner et al. (2000) within the context of non-premixed flames.

The remaining KV interaction regimes follow trends that are essentially similar to previous observations based on simple combustion chemistry models, in spite of the fundamental differences in the mechanisms for extinction due to straining, high curvature or flame-flame interactions. Based on the above observations, a revised regime diagram of KV interactions

is proposed that incorporates the new RGE regime and provides a revised delineation of the different regimes based on the role of chemistry.

Figure 5.2 shows the revised spectral diagram for the kernel-vortex interactions of hydrogen-oxygen premixed flame under stoichiometric conditions. Characteristic scales used to develop the spectral diagram are the relative measure of the tangential velocity of the vortex, $u_{\theta,\max}$, to the flame speed, S_L or $u_{\theta,\max}/S_L$ and R_v/R_f. In contrast with the previous regime diagram by Kolera-Gokula and Echekki (2007), the present diagram includes a broader range of R_v/R_f and $u_{\theta,\max}/S_L$ values. The inclusion of the RGE regime introduces non-trivial shapes for the regime boundaries, which are discussed next. At the bottom left corner of the diagram, the laminar kernel regime occupies conditions of small and weak vortices, which have limited effects on the flame kernel structure or dynamics. Above this regime is the wrinkled kernel regime, which occupies conditions of larger and stronger vortices. Wrinkled kernel regime is seen to curve behind the breakthrough regime. This happens because, although the translation speeds of the vortices are high, extremely small vortices are not able to punch through the kernel and are dissipated. The upper boundaries of this regime exhibit a positive slope. This slope is associated with the fact that for larger vortices to wrinkle the flame, they must move at a faster speed.

Above this regime is the breakthrough regime. The boundaries of this regime are relatively complex and exhibit interfaces with three regimes: 1) the wrinkled kernel regime at its lower boundaries, and 2) the global extinction and 3) the RGE regime on its upper boundaries. The global extinction regime exhibits a hyperbola-shaped lower boundary, which is bounded on

the left side by the breakthrough regime and the right side by the RGE regime. To illustrate these complex boundaries, we attempt to interpret the transitions along a line of fixed $u_{\theta,\max}/S_L$ around 150 and in the direction of increasing R_v/R_f. Starting at the breakthrough regime, increasing the vortex size imparts global straining that impacts the entire flame kernel, resulting in global extinction. As discussed earlier, global extinction results in the merging of the leading and trailing edges of the compacted flame kernel. Increasing the vortex size further transitions the interactions to the RGE regime. This transition occurs because a larger vortex enables initial contact between the kernel and the vortex only through the leading edge of the vortex. This leading edge extinguishes the central portion of the kernel, but spares the kernel edges. These edges are exposed to lower straining conditions since they are present at the periphery of the vortex pair. As the vortex intensity increases (tracing the global extinction regime upwards), the global extinction regime occupies a broader range of vortex sizes, since the kernel sees higher straining conditions and, thereby, higher likelihood of global extinction.

The RGE regime also extends to the right of the breakthrough regime, resulting in the protruding shape of the RGE regime and the presence of a “triple” point at the intersection of the wrinkled kernel, breakthrough and RGE regimes. This triple point indicates that for sufficiently large vortices, a direct transition from the wrinkled kernel regime to the RGE regime is possible without a transition through a breakthrough regime. This trend is expected since for sufficiently large vortices, as their breakthrough affects larger portions of the flame kernel resulting in almost global extinction.

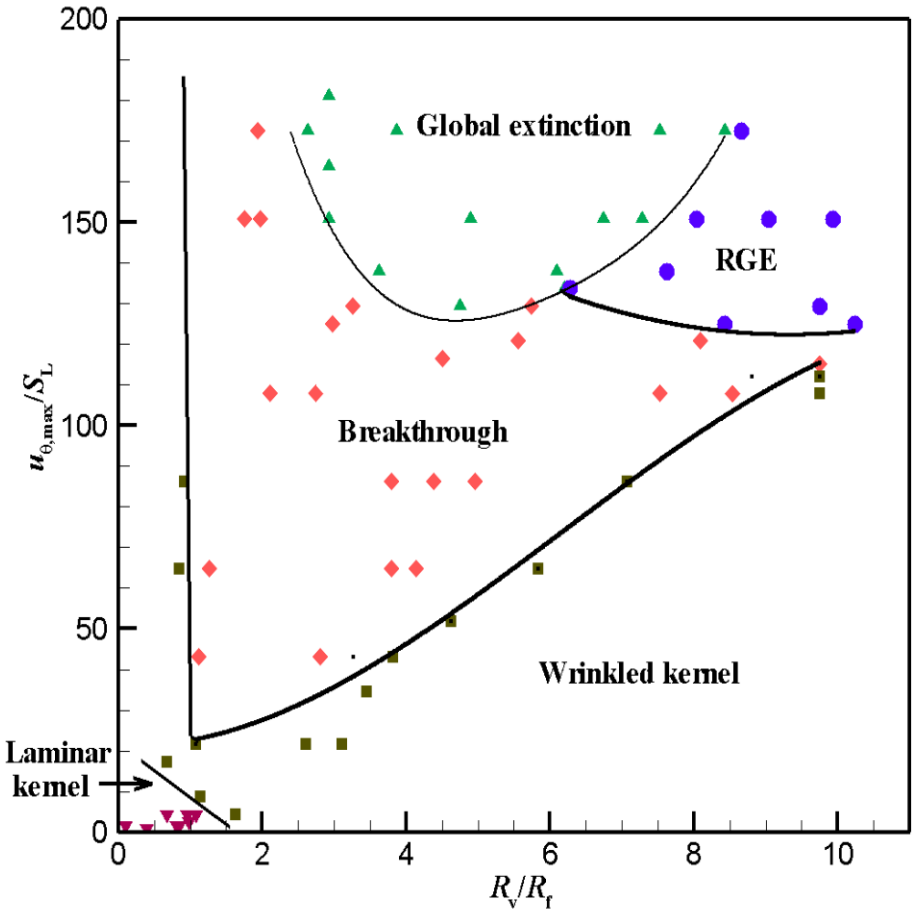

Figure 5.2: Spectral diagram for kernel-vortex interactions. Symbols: ▼ : data in the laminar kernel regime; ■ :data in the wrinkled kernel regime; ◆ : data in the breakthrough regime; ▲ : data in the global extinction regime; ● : data in the regeneration regime.

CHAPTER 6

Conclusions and Recommendations

6.1 Concluding remarks

In the present study, parametric detailed chemistry simulations of hydrogen flame kernel interactions with a vortex pair are implemented in 2D in order to explore a broad range of kernel-vortex (KV) interactions. In our simulations, we identified four regimes that have been studied experimentally by Eichenberger and Roberts (1999), Roberts and Drake (2001) and Xion and Roberts (2002) and computationally by Kolera-Gokula and Echekki (2007) and Echekki and Kolera-Gokula (2007). These regimes include: 1) the laminar kernel regime, 2) the wrinkled kernel regime, 3) the breakthrough regime, 4) the global extinction regime. In addition we identified a new, fifth regime, "regeneration after extinction" (RGE), whose phenomenology is perhaps similar to that encountered in conditions of high-intensity turbulence. These regimes exhibit relatively complex boundaries in the parameter space of vortex size and strength. It is expected that these boundaries are affected strongly by the details of the chemical model since they reflect important and sensitive balances of extinction and ignition/flame mending.

The RGE regime, in particular, enables combustion at conditions where intense turbulence results in large extinguished sections of the flame kernel. We have observed that within this regime two types of flame structures can be found. They include the standard layered flamelet structure, and more diffused reaction zone that results from the merging of multiple

flame layers. While ephemeral, this combustion mode is robust enough to support reignition of flamelet structures long after the vortex core has passed through the region. This flameless mode of combustion may indeed be relevant to the distributed reaction regime of turbulent combustion. While some degree of flame "shredding" is observed, a more important role is played by vorticity in mixing hot products and unburned reactants to sustain the combustion process.

6.2 Recommendations for Future Work

The simulations in the present study are carried out by using unity Lewis number. It would be interesting to vary the equivalence ratio of the fuel and to study its effects on the interactions. S_L can be maintained to be the same by changing the dilution. This may result in alteration of the parameters such as hydrogen consumption rate, heat release rate, temperature etc. Alterations in these parameters can govern the changes in density and viscosity near the surface of the flame. Also, there can be a shift of the interaction from one regime to another, (as seen in the case discussed in this thesis) depending on the equivalence ratio.

Instabilities such as thermo-diffusive instability, which can be studied using a expanding kernel, can be taken into account by introducing non-unity Lewis number. These instabilities can have a great impact on the expanding kernel and also can result into local and global extinction at comparatively weaker vortices. Preferential and differential diffusion may also affect the flame curvature and pocket formations that take place during the interactions.

In addition to varying the Lewis number, different sets of fuel (for example methane enriched with hydrogen) can also be studied.

REFERENCES

[1] Abdel-Gayed R. G and D. Bradley, "Combustion regimes and the straining of turbulent premixed flames," Combust. Flame **76**, 213 (1989).

[2] Borghi R., "On the structure and morphology of turbulent premixed flames," in *Recent Advances in Aerospace Sciences*, edited by C. Casci and C. Bruno _Plenum, New York, 1985, pp. 117–138.

[3] Choi W. C. and Guezennec Y. G. "Experimental investigation to study convective mixing, spatial uniformity, and cycle-to-cycle variation during the intake stroke in an IC engine," Journal of Engineering for Gas Turbines and Power Transactions of the ASME, **122**, 493 (2000).

[4] Day M. S, J. B. Bell, *Combust. Theory and Modelling* 4 (2000) 535-556.

[5] Day M, John Bell, Peer-Timo Bremer, Valerio Pascucci, Vince Beckner, Michael Lijewski, "Turbulence effects on cellular burning structures in lean premixed hydrogen flames" Combust. Flame **156** 1035 (2009).

[6] Echekki T and H. Kolera-Gokula, A regime diagram for premixed flame kernel-vortex interactions, Phys. Fluids **19**, 043604 (2007).

[7] Eichenberger D. A. and W. L. Roberts, "Effect of unsteady stretch on spark ignited flame kernel survival," Combust. Flame **118**, 469 (1999).

[8] Frenklach M, H. Wang, M. Goldenberg, G.P. Smith, D.M. Golden, C.T. Bowman, R.K. Hanson, W.C. Gardiner, V. Lissianski, GRI-Mech—An Optimized Detailed Chemical Reaction Mechanism for Methane Combustion, Tech. Rep. GRI- 95/0058, Gas Research Institute, 1995, http://www.me.berkeley.edu/gri_mech/.

[9] Kenneth K. Kuo, Principles of Combustion – second edition, John Wiley & Sons, Inc., 2005

[10] Kolera-Gokula H, Echekki T, "Direct numerical simulations of premixed flame kernel-vortex interactions in hydrogen-air mixtures" Combust. Flame **146**, Issues 1-2. pp. 155-167 (2006).

[11] Kolera-Gokula H, T. Echekki, The mechanism of unsteady downstream interactions of premixed hydrogen-air flames, Combust. Sci. Tech. **179** (2007) 2309-2334.

[12] Peters N, The turbulent burning velocity for large scale and small scale turbulence, J. Fluid Mech. **384**, 107-132 (1999).

[13] Pope, S. B., Turbulent Flows, Cambridge University Press, 2000.

[14] Ranganth B, T. Echekki, Effects of preferential and differential diffusion on the mutual annihilation of two premixed hydrogen-air flames, Combust. Theo. Model. **9** (2005) 659-672.

[15] Ratner A., J.F. Driscoll, J.M. Donbar, C.D. Carter, and J.A. Mullin, Reaction zone structure of non-premixed turbulent flames in the "intensely wrinkled" regime, Proc. Combust. Inst. **28**, 245-252 (2000).

[16] Rehm R. G, H. R. Baum, J. Res. National Bureau of Standards 83 (1978) 297-308.

[17] Rutland C.J. and Trouve A, "Direct simulations of premixed turbulent flames with non unity lewis numbers" Combust. Flame **94,** 41 (1993).

[18] Schefer R. W, Sandia National Laboratories, "Combustion of hydrogen-enriched methane in a lean premixed swirl burner", Proc. Combust. Inst. **29** (2002) 843-851.

[19] Xiong Y, W. L. Roberts, and M. C. Drake, "Investigation of pre-mixed flame-kernel/vortex interactions via high-speed imaging," Combust. Flame **126**, 1827 (2001).

[20] Xiong Y. and W. L. Roberts, "Observations on the interaction between a premixed flame kernel and a vortex of different equivalence ratio," Proc. Combust. Inst. **29**, 1687 (2002).